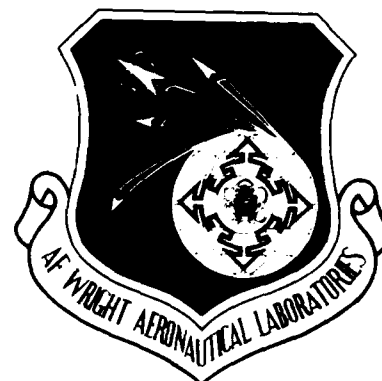AFWAL-TR-88-4176

AD-A205 185

DEVELOPMENT OF MAGNETIC FIELD ASSISTED

MELT STABILIZATION WITH HEAT AND MASS

TRANSFER CONTROL IN LOW PRESSURE

LEC GROWTH OF GaAs

Submitted by Co-Principal Investigators:

S. Motakef	Dept. of Mechanical Engineering
A.T. Patera	Dept. of Mechanical Engineering
G. Stephanopoulos	Dept. of Chemical Engineering
J. Szekely	Dept. of Materials Science & Engineering
A.F. Witt	Dept. of Materials Science & Engineering

Massachusetts Institute of Technology
77 Massachusetts Avenue
Cambridge, MA 02139

October 1988

Final Report for Period March 1984 – July 1987

Approved for public release; distribution unlimited.

MATERIALS LABORATORY
AIR FORCE WRIGHT AERONAUTICAL LABORATORIES
AIR FORCE SYSTEMS COMMAND
WRIGHT-PATTERSON AIR FORCE BASE, OHIO 45433-6533

REPORT DOCUMENTATION PAGE

Form Approved
OMB No. 0704-0188

1a REPORT SECURITY CLASSIFICATION	1b RESTRICTIVE MARKINGS
Unclassified	

2a. SECURITY CLASSIFICATION AUTHORITY	3. DISTRIBUTION / AVAILABILITY OF REPORT
2b. DECLASSIFICATION / DOWNGRADING SCHEDULE	Approved for public release; distribution is unlimited.

4. PERFORMING ORGANIZATION REPORT NUMBER(S)	5. MONITORING ORGANIZATION REPORT NUMBER(S)
	AFWAL-TR-88-4176

6a. NAME OF PERFORMING ORGANIZATION	6b. OFFICE SYMBOL (If applicable)	7a. NAME OF MONITORING ORGANIZATION
Massachusetts Institute of Technology		Materials Laboratory (AFWAL/MLPO) AF Wright Aeronautical Laboratories

6c. ADDRESS (City, State, and ZIP Code)	7b. ADDRESS (City, State, and ZIP Code)
Cambridge, MA 02139	WPAFB, OH 45433-6533

8a. NAME OF FUNDING / SPONSORING ORGANIZATION	8b. OFFICE SYMBOL (If applicable)	9. PROCUREMENT INSTRUMENT IDENTIFICATION NUMBER
AFWAL/DARPA*		F33615-83-C-5089

8c. ADDRESS (City, State, and ZIP Code)	10. SOURCE OF FUNDING NUMBERS			
	PROGRAM ELEMENT NO.	PROJECT NO.	TASK NO.	WORK UNIT ACCESSION NO.
Air Force Wright Aeronautical Labs. Air Force Systems Command Wright-Patterson AFB, OH 45433-6533	62102F	2423	01	75

11. TITLE (Include Security Classification)

Development of Magnetic Field Assisted Melt Stabilization with Heat and Mass Transfer Control in Low Pressure LEC Growth of GaAs

12. PERSONAL AUTHOR(S)

S. Motakef, A. Patera, G. Stephanopoulos, J. Szekely, A. Witt

13a. TYPE OF REPORT	13b. TIME COVERED	14. DATE OF REPORT (Year, Month, Day)	15. PAGE COUNT
FINAL	FROM 84 Mar TO 87 Jul	Oct 1988	101

16. SUPPLEMENTARY NOTATION

*Air Force Wright Aeronautical Laboratories/Defense Advanced Research Projects Agency

17. COSATI CODES			18. SUBJECT TERMS (Continue on reverse if necessary and identify by block number)
FIELD	GROUP	SUB-GROUP	
11	07		
09	01		

19. ABSTRACT (Continue on reverse if necessary and identify by block number)

The tangible output from this research effort is documented in nine theses, five patents, twenty publications in the open literature, and in thirty-six invited presentation lectures. It is also reflected in the creation of a new category of growth research capabilities which permits operation on a scale compatible with industry and establishes the basis for advanced science and technology transfer in the area of bulk crystal growth of elemental and compound semiconductors. It led to the development of a computer controlled, model-based magnetic LP-LEC facility for growth of GaAs at diameters in excess of 3 inches. In conjunction, a thermal imaging system was created which permits monitoring and control of the growth process as well as, from video-tape, the post-growth analysis of thermal field distribution and its changes. This capability makes it possible to analyze for correlations between the thermal history of a

20. DISTRIBUTION / AVAILABILITY OF ABSTRACT	21. ABSTRACT SECURITY CLASSIFICATION
☒ UNCLASSIFIED/UNLIMITED ☐ SAME AS RPT ☐ DTIC USERS	Unclassified

22a. NAME OF RESPONSIBLE INDIVIDUAL	22b. TELEPHONE (Include Area Code)	22c. OFFICE SYMBOL
Donald J. Evans	(513) 255-4474	AFWAL/MLPO

DD Form 1473, JUN 86 — Previous editions are obsolete.

19. Abstract (continued)

⟶ semiconductor and its properties. The imaging system is also an essential element for monitoring the effectiveness of heat transfer control and the viability of model-based feedforward growth control. The crystal growth research provided the background for major advances in our ability to characterize qualitatively on a micro- and macroscale the free charge carrier distribution (dopant distribution) in semiconductors. The opto-analytical approach taken provides for quantitative analyses of unprecedented spatial resolution and sensitivity within seconds and thus appears ideally suited for transfer to technology. *Liquid Encapsulated*

Czochralski S.

FOREWORD

The broad scope of the conducted research and the full spectrum of results obtained in the area of crystal growth and related subjects preclude adequate presentation in a final report. For the interested reader we therefore present listings of publications contributed to the open literature, a list of patents, and a chronicle of invited presentations given by the staff involved during the term of this contract. Insight into the accomplishments is provided through our Executive Summary and a Research Digest.

ACKNOWLEDGMENTS

CONTENTS

INTRODUCTION

The primary objectives of this research effort were directed at:

- The establishment at MIT of magnetic LP–LEC growth capability for GaAs with diameters up to 2 inches.

- The design of heat and mass transport control approaches required for optimization of LP–LEC growth with magnetic field assisted melt stabilization.

- The establishment of academic growth research activities that lend themselves to accelerated science transfer and meaningful collaboration with industry. The research effort should, moreover, provide a basis for most advanced graduate education in bulk electronic materials processing and thus contribute to curriculum development.

Motivation for the proposed work was largely in the recognition that industrial GaAs growth technology, based by necessity on proprietary empiricism, appeared only marginally able to meet existing property requirements and unable to meet property requirements for projected device technology. Broadening of the science base for semiconductor growth technology through involvement of complementary expertise in academia was considered desirable.

Primary justification for the conduct of this effort at MIT was given by available expertise in magnetic field assisted melt stabilization during Czochralski growth, an approach developed earlier in this laboratory. This approach, considered by many as

"the solution" to perfection control in melt growth of elemental and compound semiconductors, was in this laboratory considered as inadequately understood and associated with a series of predictable complications of the growth and segregation behavior. With the application of an axial magnetic field to a conventional LP–LEC GaAs growth system, the following phenomena were predicted:

- enhancement of asymmetry of the thermal field in the vicinity of the growth interface and related non–uniformity in radial segregation;

- increased thickness of critical momentum boundary layers and related segregation and interaction (crucible dissolution) effects;

- enhancement of the effects of seed and crucible rotation on growth and segregation;

- establishment of increased radial and axial thermal gradients in the melt with corresponding changes in growth behavior;

- reduction to elimination of convective heat transfer in the melt and related increased sensitivity of crystal diameter to melt temperature.

Consideration of the side effects of magnetic field assisted melt stabilization during growth of GaAs led to the identification of (a) specific issues to be resolved, (b) complementary expertise to be activated, and (c) hardware to be developed and/or acquired. Accordingly, the scope of the proposed growth research evolved into the complementary tasks:

- **Heat Transport/Control:** Temperature and temperature gradient control in the melt and the growing crystal.
  S. Motakef: *Department of Mechanical Engineering*

- **Magneto–hydrodynamics:** Forced flow control in magnetically damped, liquid encapsulated melts.
  J. Szekely: *Department of Materials Science & Engineering*
  A. Patera: *Department of Mechanical Engineering*

- **Control Theory:** Model based feedforward control driven by user dictated informal control objectives.
  R. Houpt: *Department of Mechanical Engineering*
  G. Stephanopoulos: *Department of Chemical Engineering*

- **LP–LEC Growth:** Thermal imaging; magnetic LP–LEC growth; characterization.
  A. Witt: *Department of Materials Science & Engineering*

EXECUTIVE SUMMARY

The tangible output from this research effort is documented in nine theses, five patents, twenty publications in the open literature, and in thirty-six invited presentation lectures. It is also reflected in the creation of a new category of growth research capabilities which permit operation on a scale compatible with industry and establishes the basis for advanced science and technology transfer in the area of bulk crystal growth of elemental and compound semiconductors. It led to the development of a computer controlled, model-based magnetic LP-LEC facility for growth of GaAs at diameters in excess of 3 inches. In conjunction, a thermal imaging system was created which permits monitoring and control of the growth process as well as, from video-tape, the post-growth analysis of thermal field distribution and its changes. This capability makes it possible to analyze for correlations between the thermal history of a semiconductor and its properties. The imaging system is also an essential element for monitoring the effectiveness of heat transfer control and the viability of model-based feedforward growth control. The crystal growth research provided the background for major advances in our ability to characterize qualitatively on a micro- and macroscale the free charge carrier distribution (dopant distribution) in semiconductors. The opto-analytical approach taken provides for quantitative analyses of unprecedented spatial resolution and sensitivity within seconds and thus appears ideally suited for transfer to technology.

The intangible outputs from this research effort are major and potentially more significant than those on record. The program has resulted in an interdepartmental undertaking in which faculty with complementary expertise collaborated effectively on broadening the science base for a critical area of semiconductor processing technology. This collaboration, which now also encompasses the Sloan School of Management, has a major impact on our conduct of graduate education and has a stimulating effect on our interaction with industry and the government.

DOCUMENTS GENERATED

THESES

Master's Theses

Rodammer, M.M., "Czochralski Growth of Silicon in an Axial Magnetic Field", Master's Thesis, Department of Materials Science and Engineering, September 1985.

Tarricone, L.G., "Characterization of the Optical Properties of B_2O_3 for Use in Thermal Imaging Studie3s of LEC Growth Systems", Master's Thesis, Department of Mechanical Engineeriig, September 1985.

Kelly, K.W., "Characterization and Control of Radial Heat Fluxes During Crystal Growth in Czochralski System", Master's Thesis, Department of Mechanical Engineering, June 1988.

Cao, X.Z., "LEC GaAs Crystal Growth and Characterization", Master's Thesis, Department of Materials Science and Engineeiring, expected 6/91.

Doctoral Theses

Tangborn, A., "A Direct Numerical Simulation of Czochralski Bulk Flows", Ph.D. Thesis, Department of Mechanical Engineering, September 1987.

Carlson, D.J., "The Near–Infrared Characterization of LEC Grown GaAs", Sc.D. Thesis, Department of Materials Science and Engineering, expected 9/88.

Gevelber, M.A., "Dynamics and Control of the Czochralski Process", Ph.D. Thesis, Department of Mechanical Engineering, expected 9/88.

Kelly, K.W., "Thermal Field Control of Defect Generation in GaAs Crystals Grown by the LEC Technique", Ph.D. Thesis, Department of Mechanical Engineering, in progress.

Koi, K., "Global Characterization and Control of Thermal Field in Liquid Encapsulated Systems", Ph.D. Thesis, Department of Mechanical Engineering, in progress.

PUBLICATIONS

A.F. Witt

A.F. Witt and S. Motakef, "Defect Formation and Control During LEC Growth of Compound Semiconductors", Proc. Osaka Technology Seminar '85, Osaka, Japan, June 26–27, 1985.

K.H. Yao and A.F. Witt, "Scanning Fourier Transform Infrared Spectroscopy of Carbon and Oxygen Microsegregation in Silicon", J. Crystal Growth $\underline{80}$ (2) 453-455 (1987).

A. Ostrogorsky, K.H. Yao, and A.F. Witt, "Infrared Absorbance of B_2O_3 at Temperatures to 1250°C", J. Crystal Growth $\underline{84}$ (3) 460-466 (1987).

D.J. Carlson and A.F. Witt, "Determination of Free Charge Carrier Distribution and Micro-Segregation of Dopants in n-Type GaAs", J. Crystal Growth, in press.

C. Lin, D.J. Carlson, and A.F. Witt, "Growth Related Residual Strain in LEC GaAs", J. Crystal Growth, in press.

D.J. Carlson and A.F. Witt, "Quantitative Optical Determination of Segregation in Doped Silicon: A Comparative Analysis with Spreading Resistance Measurements", J. Crystal Growth, in press.

S. Motakef

S. Motakef and A.F. Witt, "Thermoelastic Analysis of GaAs in LEC Growth Configuration, Part 1: Effect of liquid encapsulant on thermal stresses:, J. Crystal Growth $\underline{80}$, 31-50 (1987).

S. Motakef, "Thermal Conditions for Inhibition of Stress Induced Slip in Zinc-Blende Crystals in Czochralski Growth Configuration", ASME J. Appl. Mechanics $\underline{54}$, 813-821 (1987).

S. Motakef, "Thermoelastic Analysis of GaAs in LEC Growth Configuration, Part 2: Temporal evaluation on the stress field", J. Crystal Growth, in press.

S. Motakef, "Analysis of the Thermoelastic Stresses in GaAs Crystals Grown by the Bridgman-Stockbarger and the Liquid Encapsulated Czochralski Methods", Proc. ASME-WAM Conf., Boston, 1987, in press.

S. Motakef, "Thermoelastic Analysis of GaAs in LEC Growth Configuration, Part 3: Thermal conditions for control stresses", J. Crystal Growth, in review.

A.M. Cazin-Bourguignon and S. Motakef, "Thermoelastic Analysis of GaAs in LEC Growth Configuration, Part 4: Effectiveness of Various configurations for control of thermal environment", J. Crystal Growth, in review.

G. Stephanopoulos

M.A. Gevelber, G. Stephanopoulos, and M.J. Wargo, "Dynamics and Control of the Czochralski Process, Part 1: Modelling and dynamic characterization", J. Crystal Growth $\underline{84}$. 647 (1987).

M.A. Gevelber, M.J. Wargo, and G. Stephanopoulos, "Advanced Control Design Consideration for the Czochralski Process", J. Crystal Growth 85, 256 (1987).

M.A. Gevelber, G. Stephanopoulos, and M.J. Wargo, "Dynamics and Control of the Czochralski Process, Part 2: Objectives and control structure design", J. Crystal Growth, accepted for publication.

J. Szekely

R.A. Cartwright, N. El-Kaddah, and J. Szekely, "The Effect of an Axial Magnetic Field at the Interface of a Crystal Grown by the Czochralski Method", IMA J. Appl. Math. 35, 175 (1985).

R.A. Cartwright, D.T.J. Hurle, R.W. Series, and J. Szekely, "The Influence of Crucible Rotation on the Effective Distribution Coefficient in Magnetic Czochralski Growth", J. Crystal Growth (1987).

O.J. Ilegbusi, J. Szekely, and R.A. Cartwright, "Some Asymptotic and Computed Results on Magnetically Damped Czochralski Crystal Growing Systems", J. Physicochemical Hydrodynamics 10 (1) 33-51 (1988).

O.J. Ilegbusi, J. Szekely, and R. Cartwright, "An Order of Magnitude Approximation and its Numerical Verification of Magnetically Damped CZ Growth Systems", accepted for publication in J. Crystal Growth.

PATENTS

Filed:

Motakef, S.: "Heat Transfer Control During Crystal Growth", Serial No. 61,117, filed 6/10/87, MIT Case No. 4234.

Gevelber, M.A., and Stephanopoulos, G.: "Interface, Melt and Crystal Control System for the Czochralski Process: Control of Segregation, Dislocation, Formation, and Shape", Serial No. 072,554, filed 7/13/87, MIT Case No. 4408.

Ostrogorsky, A.: "Method and Apparatus for Single Crystal Pulling Downwardly from the Lower Surface of a Floating Melt", Serial No. 112,499, filed 10/22/87, MIT Case No. 4443.

Not Yet Filed:

Gevelber, M.A., and Patera, A.T.: "Interface Angle Estimation System", MIT Case No. 4447.

Submitted during subsequent contract period; not yet filed:

Carlson, D.J.: "Measurement System for Micro-Distribution of Free Charge Carriers in Compound Semiconductors", MIT Case No. 4626.

PRESENTATIONS

A.F. Witt

"Advanced Electronic Materials in High Technology", Departmental Open House, MIT, Cambridge, MA, April 4, 1984.

"New Approaches to Growth of Advanced Electronic Materials for Device Fabrication", Grumman Aerospace Corporation, Bethpage, NY, May 10, 1984.

"Production of Electronic Materials: Status and Projected Needs", ILP for SOHIO, MIT, September 5, 1984.

"Solidification from the Melt", American Society for Metals, Materials Science Seminar on "Advances in Electronic Materials", Detroit, MI, September 15, 1984.

"Composition and Defect Control During LEC Growth of GaAs", SEMICON East '84, Bayside Exposition Center, Boston, MA, September 19, 1984.

"On Social Awareness of Engineering Professionals", MIT Chapter Tau Beta Pi, MIT, October 3, 1984.

"Overview of Electronic Materials Processing at MIT with Emphasis on Silicon Crystal Growth and Analysis", Xerox Corporation, Webster, NY, November 12, 1984.

"New Outlook on Control of Crystalline and Chemical Perfection During Growth of Silicon", San Diego, CA, December 3, 1984.

"New Approaches to Growth of GaAs for Device Fabrication", SEMICON/New York, New York City, NY, December 14, 1984.

"On the Significance of Heat and Mass Transfer Control during Electronic Materials Processing in Reduced Gravity Environment", Astronaut Mini-Lecture, Lyndon B. Johnson Space Flight Center, Houston, TX, January 22, 1985.

"Chemistry: The Missing Link in the Advancement of Electronic Materials", Department of Chemistry Seminar, North Carolina State University, Raleigh, NC, February 18, 1985.

"New Development in Processing of Electronic Materials", Workshop on Surface Modification Technology, Sponsored by Combustion Engineering, Inc., and Spire Corporation, Sonesta Hotel, Cambridge, MA, April 2, 1985.

"Problems with Semiconductors", Undergraduate Materials Society, MIT, Cambridge, MA, April 25, 1985.

"Low-Pressure LEC Growth of GaAs", GaAs Technology Review, DARPA, McLean, VA, May 2, 1985.

"Defect Formation and Control During LEC Growth of Compound Semiconductors", with S. Motakef, Osaka Technology Seminar '85, SEMICON/Osaka, Osaka, Japan, June 27, 1985.

"University/Industry Interactive Research in Electronic Materials", University of Sao Paulo, Brazil, July 25, 1985.

"Crystal Growth", Space Commercialization Consortium Meeting, Materials Processing Center, MIT, October 10, 1985.

"Growth and Characterization of Large-Diameter Semiconductor Single Crystals", with S. Motakef, A. Patera, J. Szekely, and G. Stephanopoulos, Fall 1985 VLSI Research Review, Microsystems Research Center, MIT, December 16, 1985.

"Development of Magnetic Field Assisted Melt Stabilization with Heat and Mass Transfer Control in Low Pressure LEC Growth of GaAs", DARPA GaAs Technology Review, Washington, DC, April 30, 1986.

"Semiconductor Single Crystal Growth", Materials Processing Center, Spring Workshop on Advanced Materials and Processing, MIT, May 8, 1986.

"Advanced Electronic Materials and the Potential of Reduced Gravity Environment", Jet Propulsion Laboratory, Pasadena, CA, May 14, 1986.

"New Approaches to the Growth of GaAs", Distinguished Lecture Series, Center for Advanced Materials, University of California, Berkeley, CA, February 18, 1987.

"Development of New Control Systems for Growth of Silicon", Nippon Research Review Meeting, ILP, MIT, March 9, 1987.

"New Approaches to Processing of Advanced Compound Semiconductor Materials", GTE Laboratories, Waltham, MA, March 16, 1987.

"Oxygen Control in Czochralski-Type Silicon", Monsanto Electronic Materials Advisory Board Symposium, Milton Keynes, England, July 14, 1987.

"Systems Control by Thermal Imaging During LEC Growth of GaAs", with M.J. Wargo, S. Motakef, and M.A. Gevelber, ACCG-7, Monterey, CA, July 16, 1987.

S. Motakef

"Thermoelastic Analysis of GaAs Crystals in LEC Growth Configuration: Optimum Thermal Characteristics of the Growth Environment", Ferrofluidics Corp., Nashua, NH, January 1986.

"Influence of Liquid Encapsulant on Generation of Thermal Stresses in GaAs Crystals Grown by the LEC Technique", American Association for Crystal Growth, Boston, MA, September 1986.

"Heat Transfer Control During LEC Growth of GaAs", 1st Workshop on Bulk Crystal Growth, Arizona State University, Tempe, AZ, November 1986.

"Modelling of Crystal Growth Systems", Air Force Wright-Patterson Materials Laboratory, Workshop on Modelling of Materials Processing, Dayton, OH, January 1987.

"Heat Transfer Control During LEC Growth of GaAs", Workshop on Bulk Crystal Growth, MIT, Cambridge, MA, April 1987.

G. Stephanopoulos

"Dynamics and Control Design for the Czochralski Process", by M.A. Gevelber, New England Section of the American Associate for Crystal Growth, Boston, MA, May 1987.

"Control Design Consideration for the Czochralski Process", with M.A. Gevelber, General Electric Corporate Research & Development, Control Division, Schenectady, NY, September 1987.

"Reduced-Order Model in the Design of Control Algorithm for LEC Growth of GaAs", with M.A. Gevelber, A.I.Ch.E. Annual Conference, NY, November 1987.

J. Szekely

"The Mathematical Modelling of Melt Flow in Magnetically Damped CZ Systems", with R. Cartwright, A Conference on the Modelling of Crystal Growing Systems, Oxford, England, 1984.

"The Modelling of Magnetically Damped CZ Growth Systems", Annual Meeting of A.I.M.E., 1986.

FACILITIES

An essential element of this research undertaking was collaboration on LP–LEC

growth of GaAs with industry and science transfer to industry. The realization of this

objective demanded a fundamental departure from conventional academic crystal

growth research. It required the acquisition and operation of industrial–scale facilities

for growth, post–growth processing, and analysis, and commensurate space. The

Institute built for this project, according to specifications, a growth laboratory (Fig. 1),

and made a characterization laboratory (Fig. 2) and a processing laboratory

available. The primary growth and processing facilities acquired through

DARPA/AFWP enjoyed vital complementary support by industry. Most significant were

the contributions by:

> AT&T (Western Electric)
> MA/Com
> Monsanto Electronic Materials Corporation
> Motorola, Inc.
> North American Philips
> RCA
> Spectrum Technology, Inc.
> Texas Instruments, Inc.

and by the government:

> University Research Instrumentation Program (URIP)
> NASA

The broad support base permitted installation and operation of four growth systems,

of which one is dedicated to magnetic LP–LEC growth of GaAs, and one to the

development of heat transfer control systems and the building of a data base. A

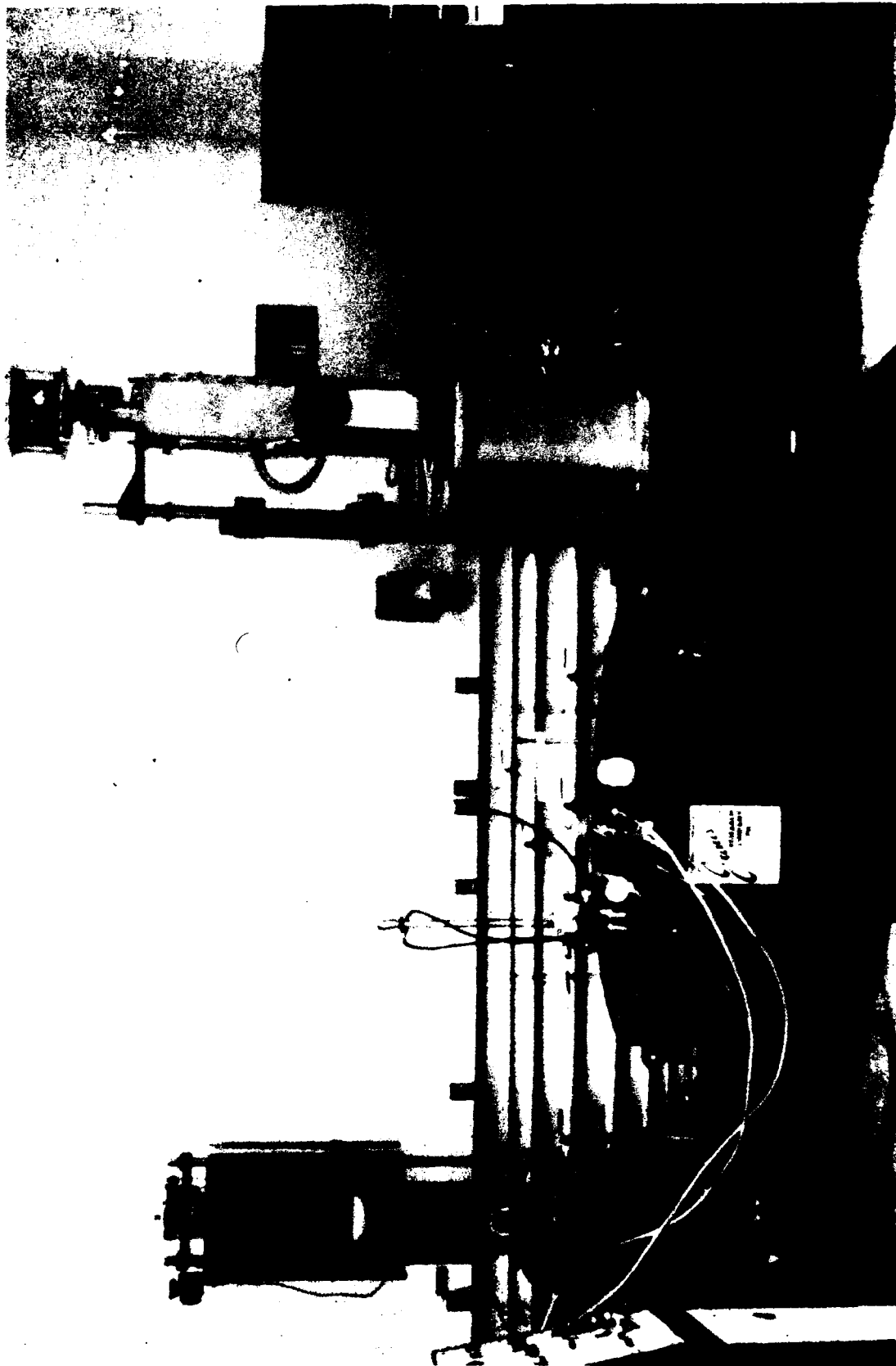Hamco CG–2000 system was used to test prototype control systems, including

Fig. 1 LP–LEC facility (left) and Silicon Growth Facility (right). The superconducting magnet (middle) is transferable via an overhead chain hoist to either of the growth systems.
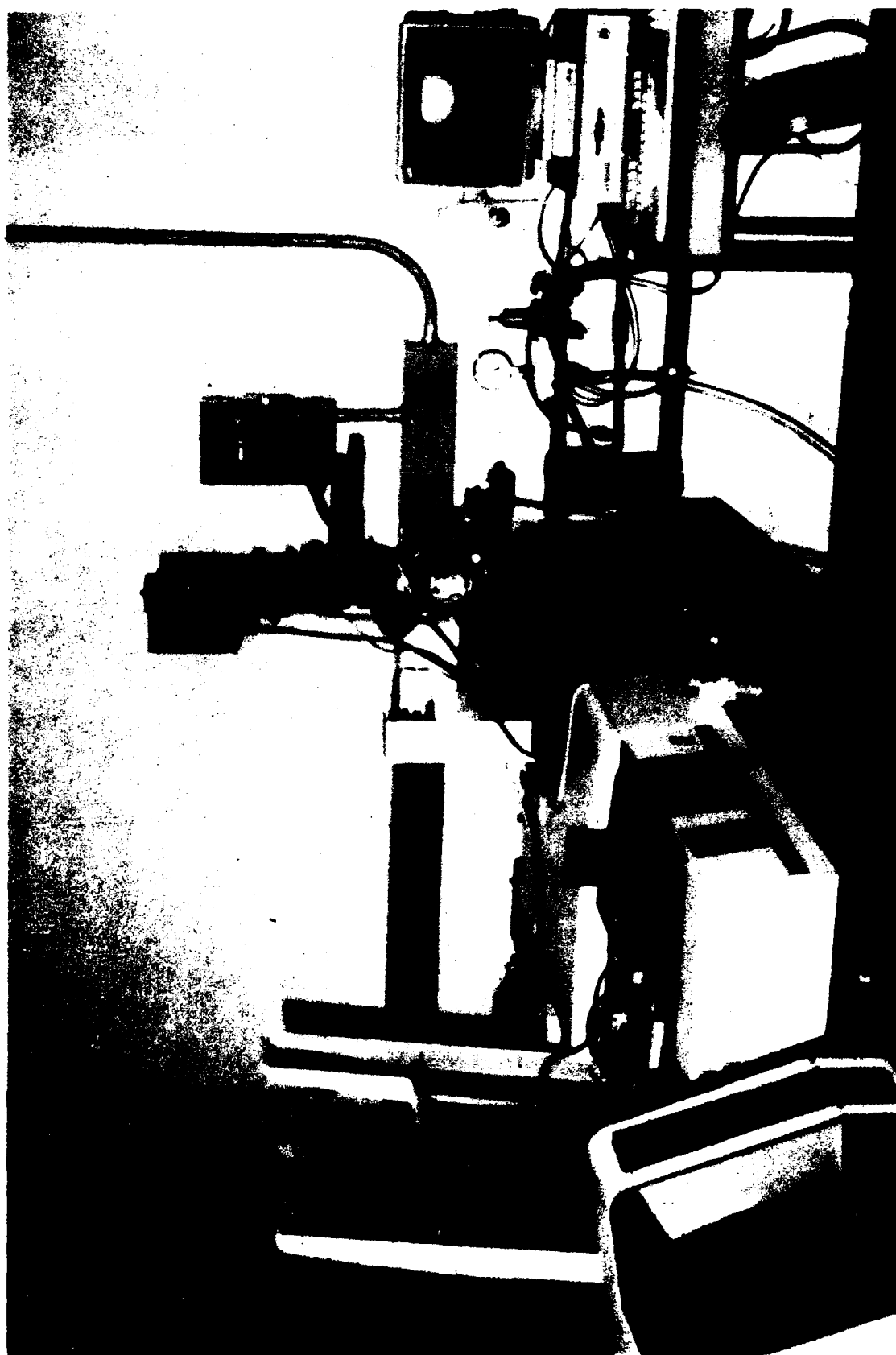
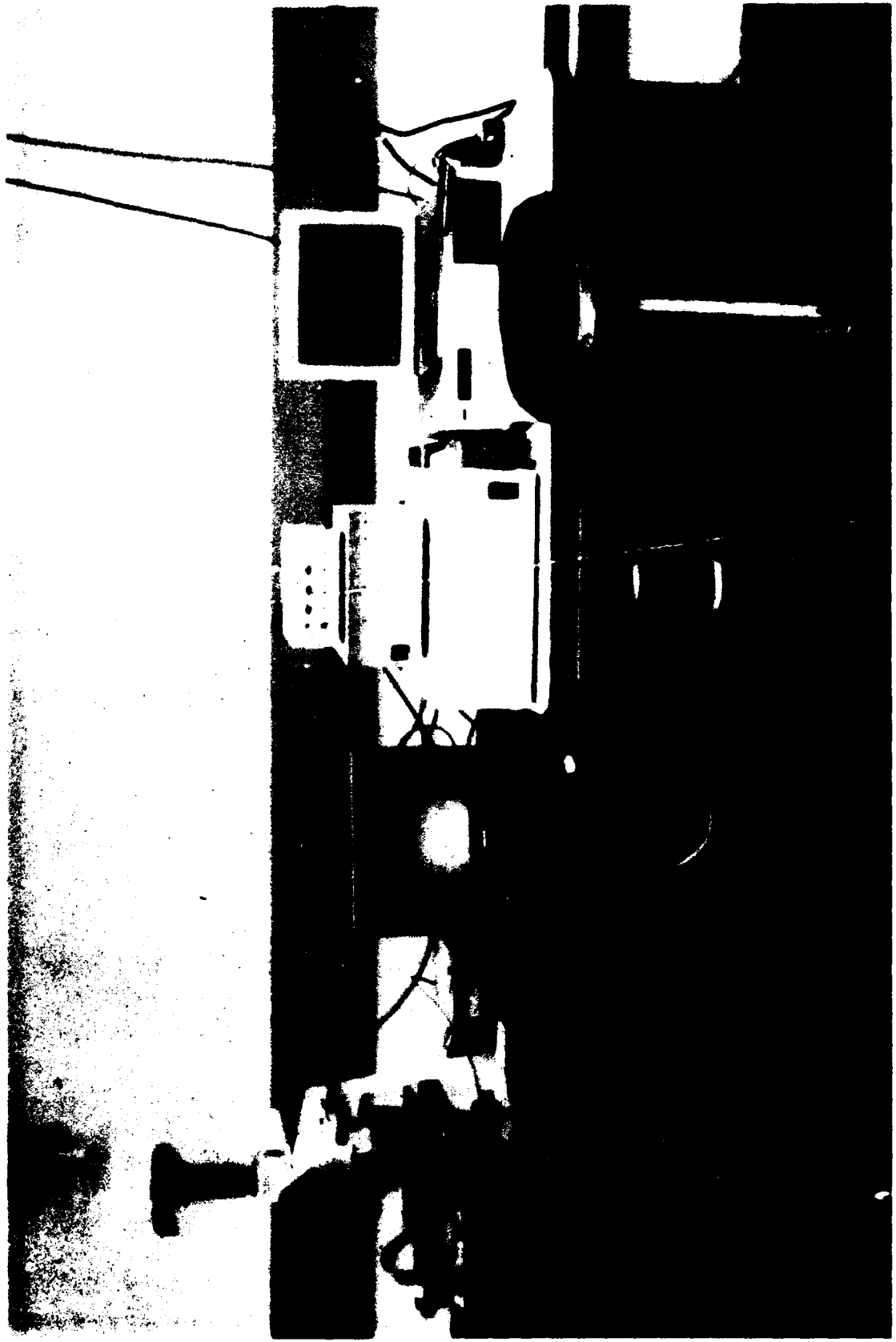Fig. 2a   Fourier Transform IR Facility with scanning IR microscope.

Fig. 2b   NIR Scanning Facility.

thermal imaging on growth of dislocation free silicon with diameters of up to 5–inches. A most recently acquired Hamco CG–800 puller (Spectrum Technology, Inc.) is continuously being modified (installation of monitoring sensors and control activators) for implementation of computer–operated, model–based feedforward growth control.

The experimental approach to magnetic field assisted melt stabilization was guided largely by symmetry considerations and by the desirability of one magnet serving several facilities. These boundary conditions and the necessity of power stability for computational operations resulted in the design of a "portable" superconducting magnet with 42–inch bore yielding a maximum vertical field of 6 kGauss (American Magnetics Corporation). In persistence mode, the cryogenics consumption is in average 100 ml of LHe which provides for about three months of continuous operation without refill.

The computational center of the growth facility (Fig. 3) consists of a Mass Comp MC–5500 with high speed data acquisition and control capability. The MC–5500 also accommodates an RTI (Recognition Technology, Inc.) image processing subsystem used for thermal imaging and growth control as well as for quantitative optical (NIR) analysis of GaAs. The analytical facilities available for this effort ranged from chemical etching and microscopy to FFTIR and photo–luminescence spectroscopy, optical absorption analysis, X–ray topography,

Fig. 3　Computational Center of LP–LEC Growth Facility.

optical strain analysis and Hall effect analysis. Crystal processing facilities included wafer cutting, lapping, polishing and etching.

To achieve desired integration of the theory-oriented modelling groups with the experimental activities, bi-weekly common seminars were held and all groups were "interconnected" via the Ethernet network. Individuals involved in modelling had the opportunity to assist in growth experiments and analyses as desired.

RESEARCH DIGEST

1. HEAT TRANSPORT/CONTROL

HEAT TRANSFER CONTROL

This research effort was focused on identification and control of parameters influencing the plastic deformation and dislocation generation during LEC growth of GaAs. The work included thermal modelling of the growth system as well as hardware development for control of stresses in the growing solid.

Thermoelastic Modelling of the LEC Growth System

Thermal Transparency of the Encapsulant:

The effect of transparency of the boric oxide encapsulant to infrared radiation was studied by numerical simulation of the governing energy and linear thermoelastic equations. As thermophysical properties on IR-transmittance of boric oxide were not available at the time of the study, the analysis was conducted for two limiting cases of thermally transparent and opaque encapsulants. The results indicated that the thermal transparency of the encapsulant has an overriding influence on both the maximum stresses experienced by the crystal as well as the location of their occurrence (Fig. 1.1). For an opaque encapsulant, we found that the crystal experiences excessive stresses as it emerges from the encapsulant. These stresses exceeded the critical resolved shear stress (CRSS) of the matrix by a factor of close to 10. Increasing the encapsulant thickness resulted in reduction of the "thermal
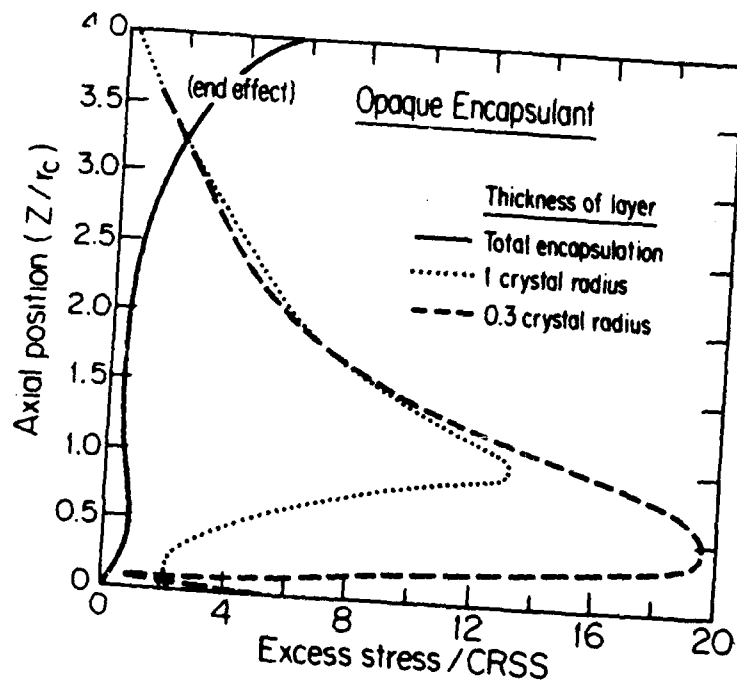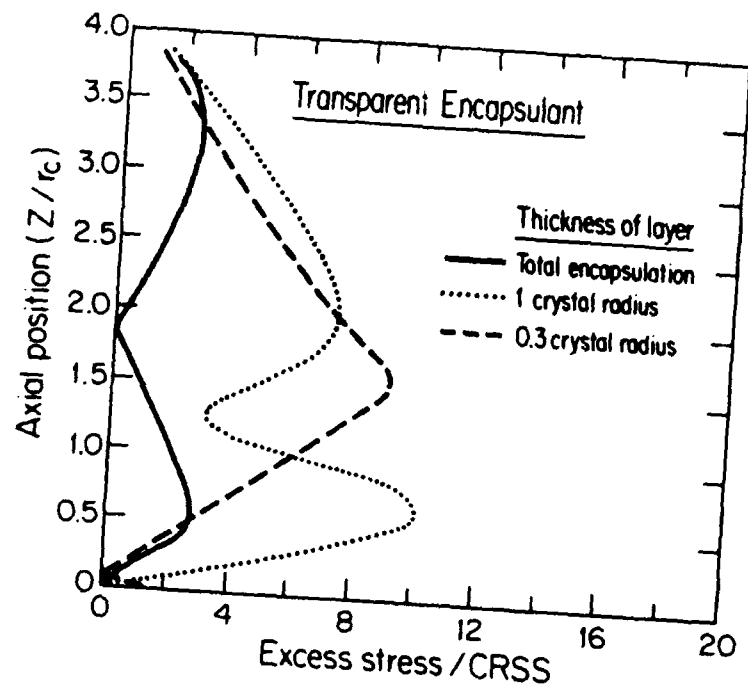
Fig. 1.1   The influence of infrared transparency and thickness of liquid encapsulant on excess stresses in a 3-inch GaAs crystal.

shock" experienced by the crystal as it emerges from the encapsulant. For a transparent encapsulant, elastic stresses in excess of CRSS of the crystal occurred by overheating of the lower portion of the crystal and excessive cooling of its upper parts. In this situation, increasing the encapsulant thickness resulted in increased stresses in the lower parts of the crystal. The analysis indicated that approaches to control of stresses in the growing crystal require quantification of the IR-transmittance properties of boric oxide at elevated temperatures. This finding led to the experimental measurement of the absorption coefficient of the encapsulant by FTIR techniques.

This study was published in the Journal of Crystal Growth 80, 37 (1987).

Convection in the Encapsulant:

An outstanding issue in the effect of the boric oxide on stress generation in the crystal was the effect of convection in the encapsulant. A.S. Jordan and colleagues [1] had attributed the primary mechanism for stress generation in the growing solid to convection in the encapsulant. As the heat transfer mechanism and correlation used in that study were not accurate, the effect of natural convection in the boric oxide on heat transfer from the crystal and stress generation in the solid was studied by numerical simulation of energy and thermoelastic equations in the solid and Navier-Stokes and energy equations in the encapsulant for both limits of opaque and transparent encapsulants. The results indicate that convection in the boric oxide plays

a minor role in heat transfer from the crystal for both limits of encapsulant IR-transparency, and, thus, conclusions derived from the assumption of significant convection in the melt are incorrect.

This study was published in the International Journal of Heat and Mass Transfer 30 (7) 1487-1495 (1987).

Thermoelastic Modelling of the LEC Growth System:

The above analyses indicated that accurate quantification of the thermal field in the growth system is a prerequisite to the unambiguous understanding of the parameters controlling the growth dynamics and stress generation in the growing crystal. Thus, a detailed package for simulation of the thermal field in the LEC system based on a 6-inch hot zone (presently used in our laboratories for growth of GaAs) was developed. In this simulation package the radiative interaction between various surfaces in the growth system are accurately modelled using the available thermophysical properties, and the growth interface shape is calculated by including the relationship between the meniscus shape and crystal diameter with parametric dependence on pull rate and heater power. The heat transfer in the boric oxide is modelled as a semi-transparent medium with a spectral absorption coefficient. The simulation package includes all details of the growth system from a resistive heater to the presence of the water-cooled shaft supporting the crucible assembly (Fig. 1.2). This tool enables us to establish a one-to-one relationship between experimental
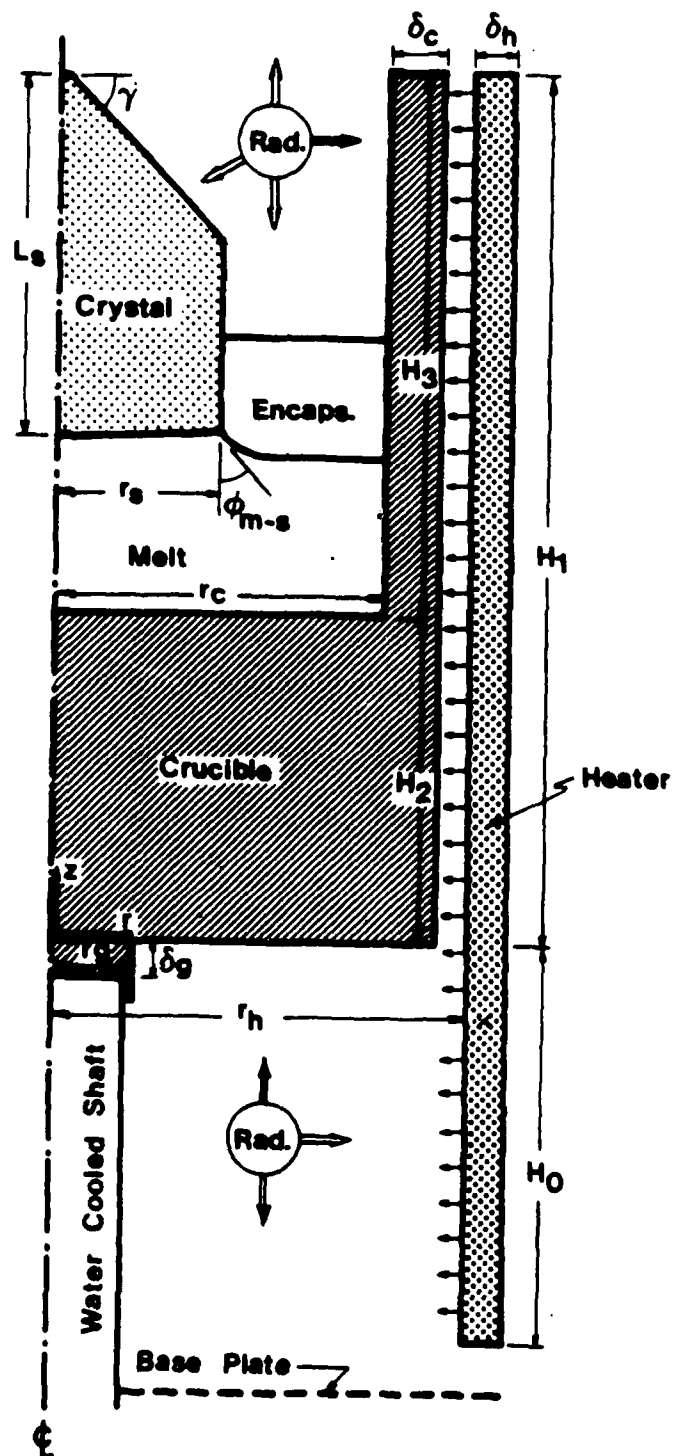
Fig. 1.2   The model of growth systems used in numerical simulation of LEC growth of GaAs.

efforts and simulation results, and is presently in use for simulation of magnetic LEC GaAs and magnetic Czochralski Si growth. This package was used, for the first time, to accurately quantify the stresses in crystals grown in our LP–LEC system, and to investigate the effectiveness of various approaches to control of thermal stresses in the solid. A series of simulation studies revealed the significant role played by the morphology of the growth interface in generatior. of stresses in the crystal where, depending on the pull rate, stresses larger than those experienced by the crystal during emergence from boric oxide are generated (Fig. 1.3). This study also showed the inadequacy of constant diameter growth as a control objective where two constant diameter crystals grown at different pull rates were shown to experience drastically different stresses (Fig. 1.4). Thus, in addition to control of heat transfer from the growing solid, control of the nonplanarity of the growth interface appears to be mandatory in attempts at reducing stresses in the crystal.

Part of this study has been published in the Journal of Crystal __88__ 341 (1987).

Control of Stresses:

The parameter space for control of stresses during LEC growth of GaAs was identified on a fundamental basis by considering the parameters influencing the stress field in the crystal. In this study the crystal was considered independently of its growth environment, and the thermal conditions necessary for maintaining stresses in the crystal at below CRSS of the matrix were identified. The control parameter
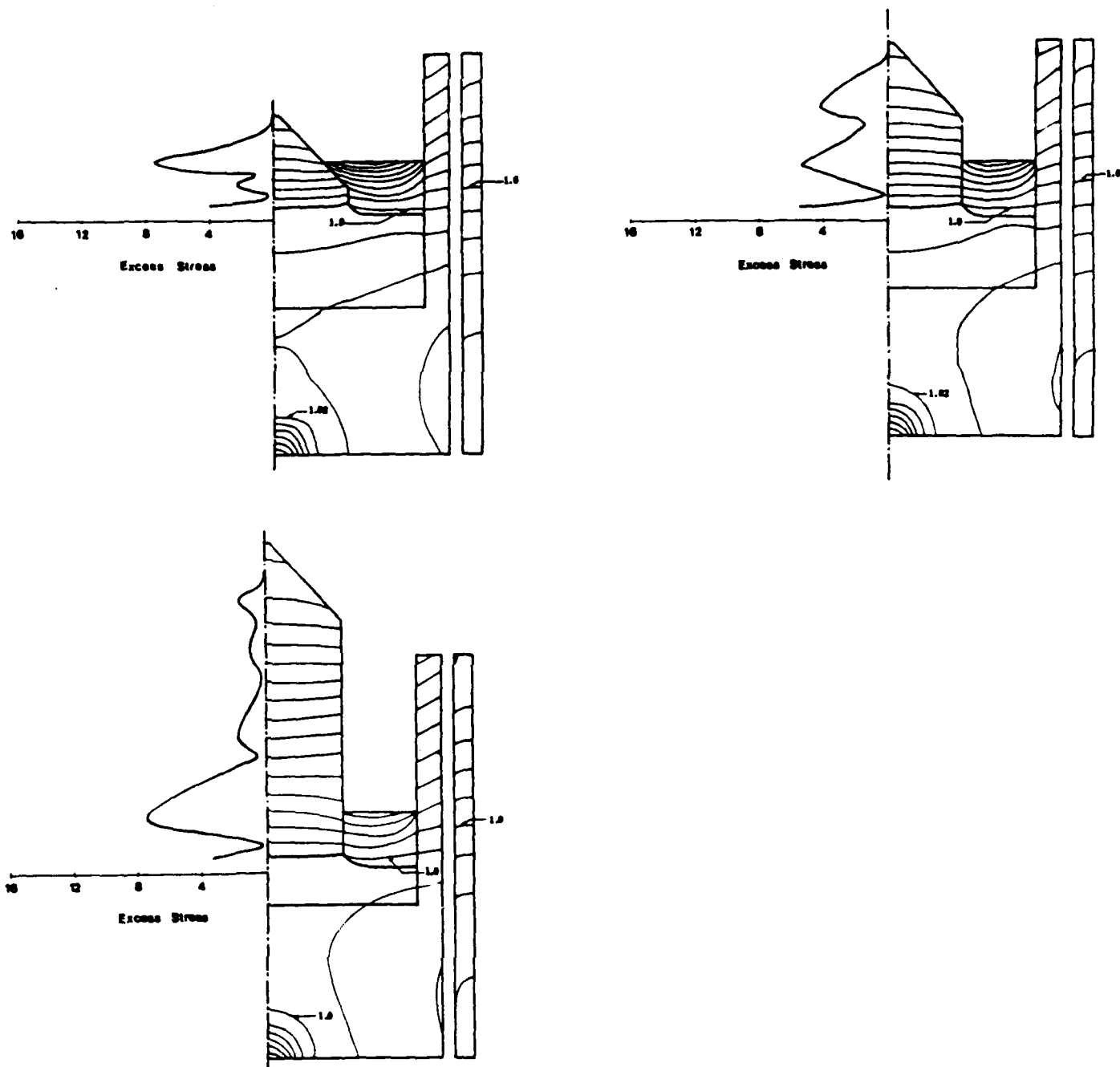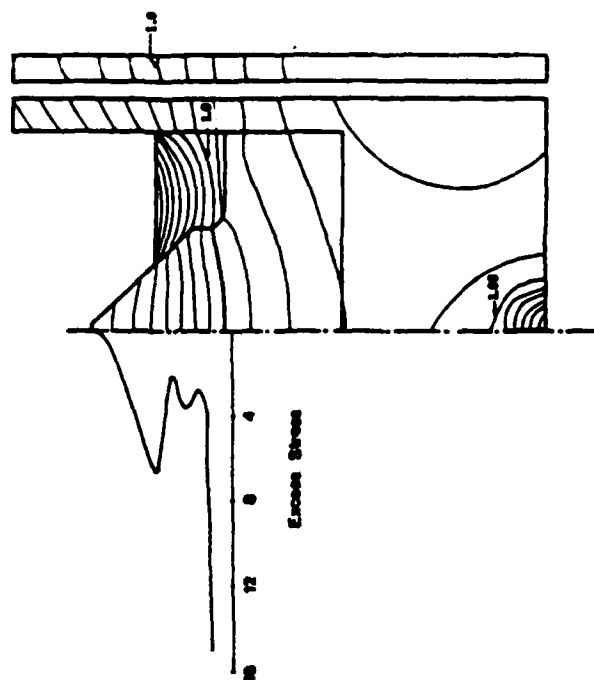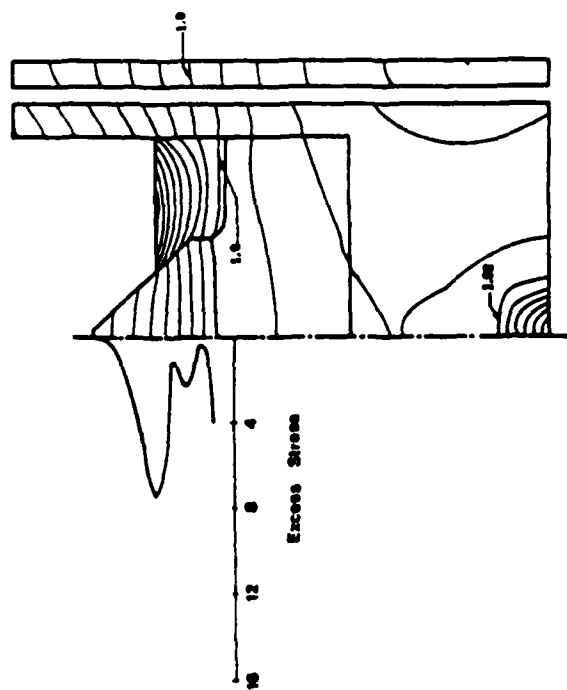
Fig. 1.3   The temperature field in the growth system and the axial distribution of excess stresses at various stages of growth of 3-inch GaAs crystals.

GROWTH RATE = 2 cm/hr

GROWTH RATE = 0.2 cm/hr

Fig. 1.4   The effect of pull rate on the stresses generated at the growth interface during constant diameter growth of GaAs.

space was not linked to conventional LEC growth systems; thus, it provided the rational basis for hardware development and modification of conventional systems. This analysis indicated that the primary controlling parameter during the early stages of growth are cone geometry and solid–liquid interface shape. As the crystal length exceeds two crystal radii, heat transfer at its periphery becomes the dominant factor. Maximum allowable heat transfer rates at the crystal periphery required to maintain the stresses in the crystal at below the plasticity limit of the matrix were calculated and were exceedingly small compared to heat loss from the crystal cone. These results suggest that the primary heat loss from the crystal, in an optimum growth condition, is radiative loss from the crystal top and the crystal side should be, essentially, maintained adiabatic. This finding indicates that controlling the stresses in the crystal should not be considered only through approaches taken where, by passive heat shields or direct RF heating, heat transfer from the crystal is reduced, but special attention should also be paid to avoid excessive heating of the crystal. This analysis unambiguously established that the optimum approach to control of heat transfer from the crystal is to actively control the growth environment within very restrictive bounds. These findings were incorporated into the design of the Heat Transfer Control System (HTCS).

This study was published in the Journal of Applied Mechanics 54, 813–821 (1987).

Thermoelastic Study of GaAs in Bridgman–Stockbarger
Growth Configuration:

The results of our experimental and modelling studies of the LEC system demonstrated that the primary source of inadequacy on controllability of the thermal field in GaAs crystals grown in this configuration stems from the transient nature of the growth process and the complex thermal coupling between the crystal, encapsulant, and the crucible walls. Thus, we conducted a modelling study of the Bridgman–Stockbarger growth system: by controlling the "hot" and "cold" zone temperatures, the growth interface can thus be located inside an adiabatic region (necessary condition established by our modelling results described above), and the interface shape can be controlled effectively by controlling the location of the solidification front in the gradient zone (Fig. 1.5). Our analysis established that, by proper choice of hot and cold zone temperatures and furnace geometry, stresses in the crystal can be easily maintained below the plasticity limit of the matrix. As part of this analysis, the effect of the wetting of the charge by the crucible was studied; adhesion of the crystal to the crucible during growth will result in generation of stresses that will exceed thermal stresses close to 50 times (Fig. 1.6). The influence of the crucible material on the morphology of the growth interface as well as the possible wetting of the charge suggest that the primary issue in growth of larger diameter GaAs crystals by the Bridgman–Stockbarger system is the identification of a
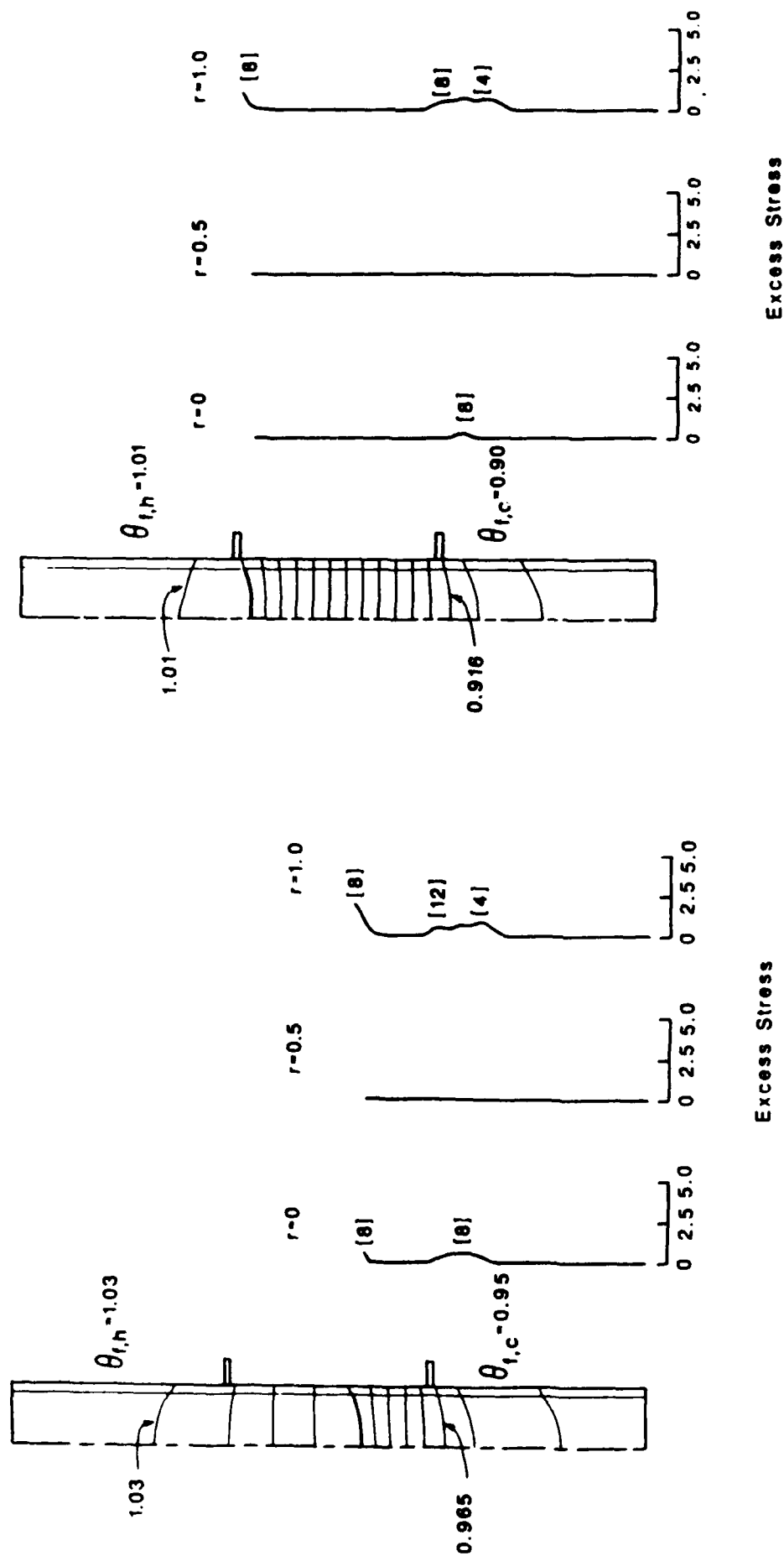
Fig. 1.5 Excess stresses in 3-inch GaAs crystals grown by the Bridgman–Stockbarger technique. Reduction of the interface nonplanarity through adjustment of furnace temperature leads to near elimination of excess stresses in the crystal.
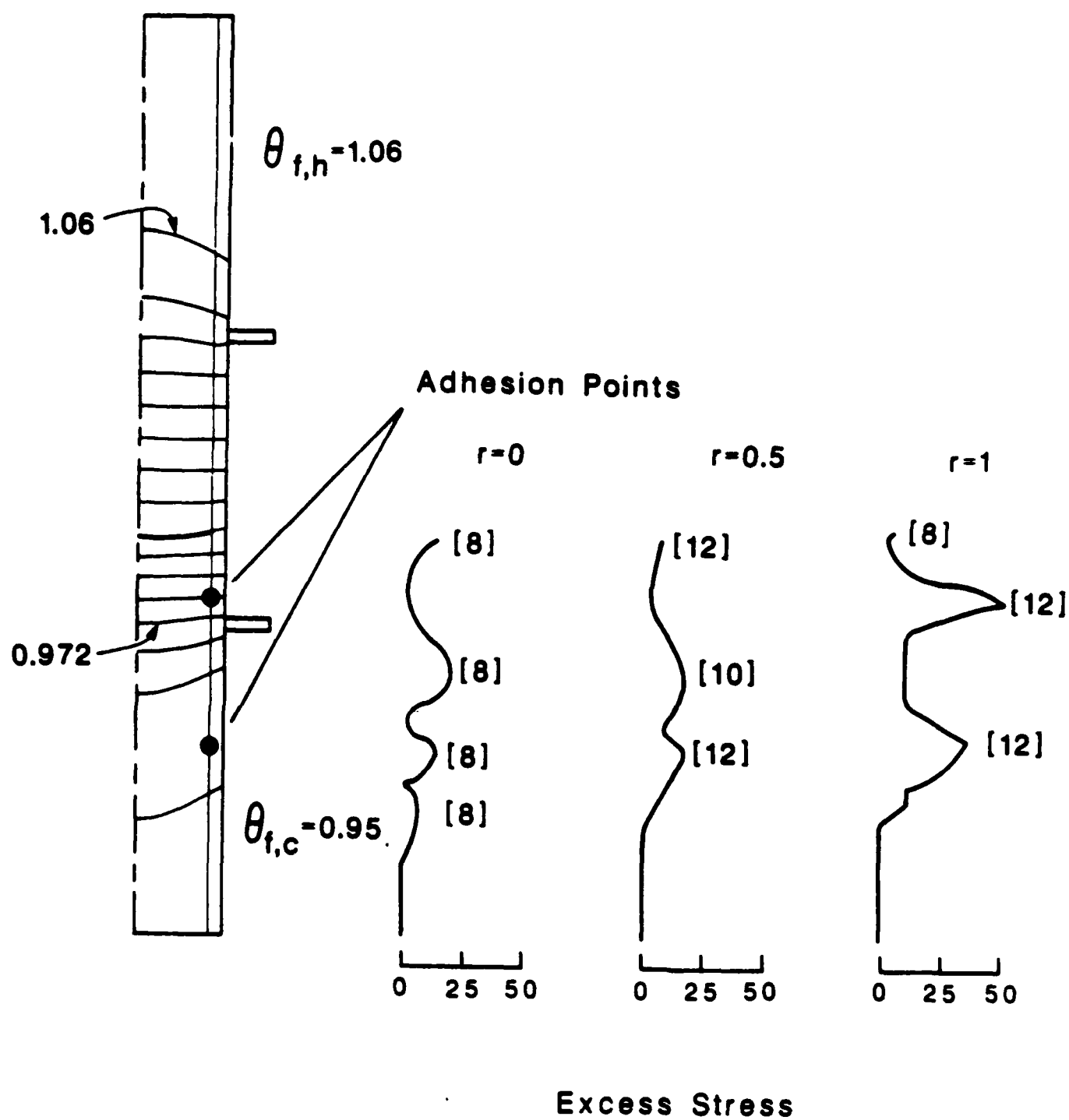
Fig. 1.6   Effect of charge wetting on stress distribution in the crystal.

nonwetting crucible material with the proper thermal conductivity and thickness to minimize the deleterious effect of crucible on interface morphology.

This work has been published in the Proceedings of the ASME Winter Annual Winter Meeting, WA/HT-2, Boston, MA, 1987.

Design and Construction of Active Heat Transfer Control System

In this facet of the research project, an active heat transfer control system was designed and built to control the heat transfer from the growing crystal at limits established by the modelling study. The primary objective of the HTCS is establishment of controllability of the thermal environment around the growing crystal by controlling heat transfer from the crystal. This approach is fundamentally different from approaches where the temperature of the growth environment is the control variable. The reason for this departure from the conventional, and more intuitive, approach is related to two issues. First, the modelling results indicate that, using currently accepted values of CRSS as the threshold stress values for massive onset of dislocation generation, the heat transfer from the crystal side should be maintained at very low values. This would indicate that the axial variation of the environmental temperatures has to be maintained nearly linear, which, considering the coupled heat transfer in the LEC system, is presently considered to be impractical. Second, accurate quantification of the environmental temperature requires an accurate thermophysical data base (primarily surface radiative properties) for the crystal and its

environment as well as a means to quantify the variation of these parameters during growth. Considering the calculated restrictive bounds on the maximum allowable heat transfer rates from the crystal and the strong thermal coupling between the crystal and its environment, errors associated with the thermophysical properties would significantly influence the temperature field in the crystal.

The first system built was based on the conventional wisdom that excessive heat transfer from the crystal is the major source of stress generation, and thus the system was built to control heat transfer from the growing solid. The HTCS consists of five isolated modules stacked on top of each other (Fig. 1.7). Each module consists of a high thermal conductivity shaped material (nickel) which is separated from the zone's heater by a thermal insulation. The temperature drop across the layer of insulation is measured and used as the indicator for the magnitude of heat transferred through the module. By adjusting the heater power, the temperature drop across the insulation – and, thus, the heat loss from the crystal – can be controlled. Upon completion of the HTCS and its installation in a growth system, it was discovered, unexpectedly, that for various growth configurations the lower portion of the crystal was excessively heated, and not cooled, by its environment. These observations were also corroborated by modelling results (Fig. 1.8).

In order to unambiguously establish the various modes of heat transfer into and out of the crystal, physical modelling experiments were conducted using graphite and
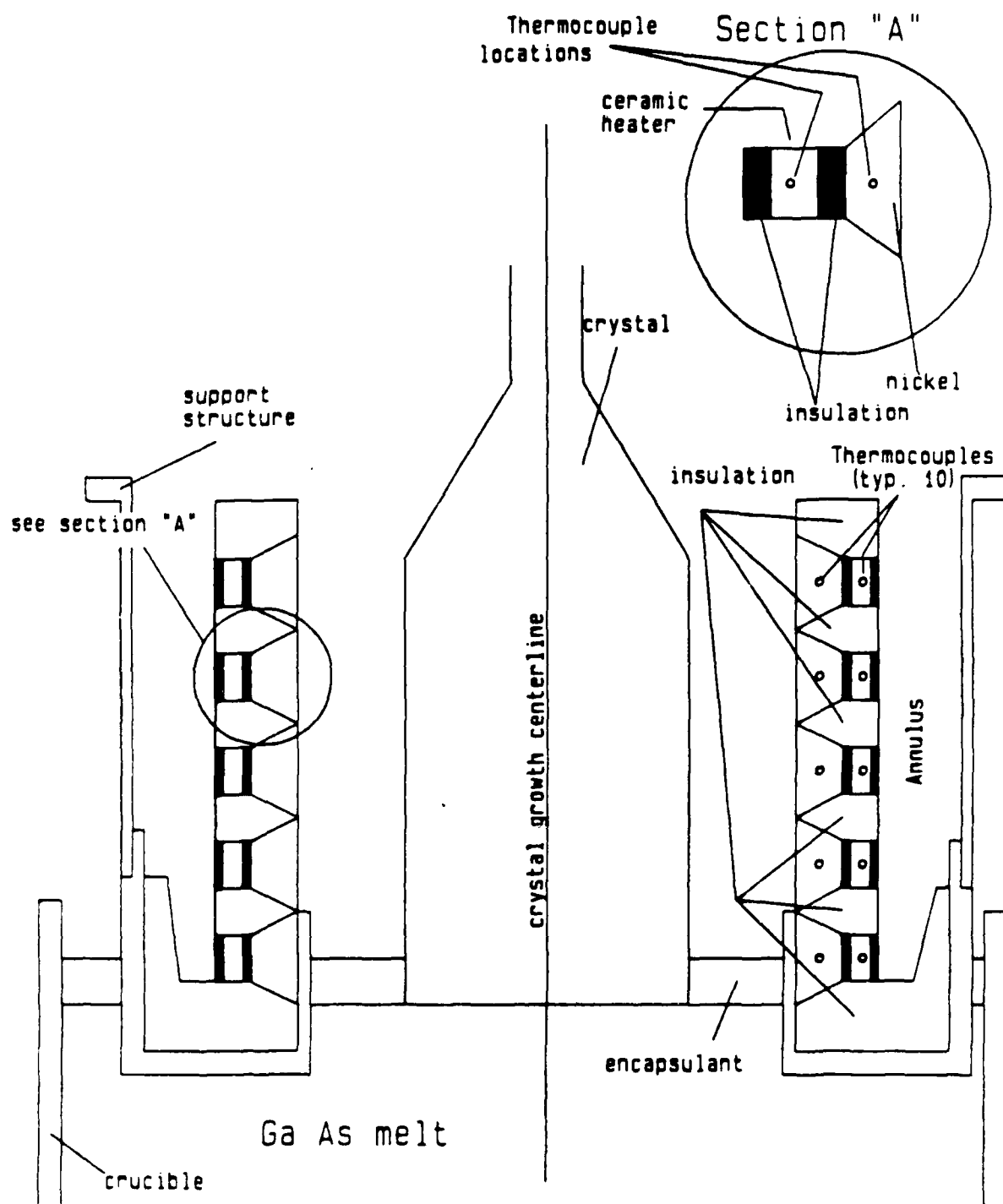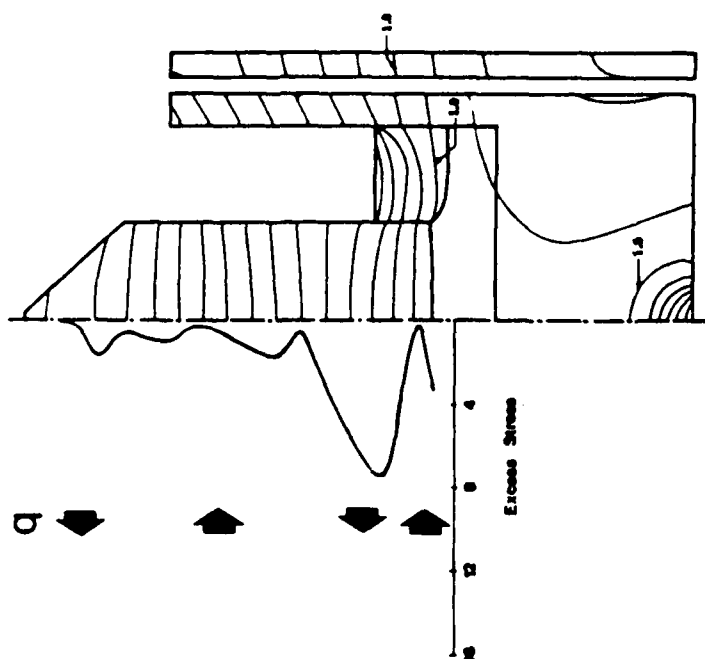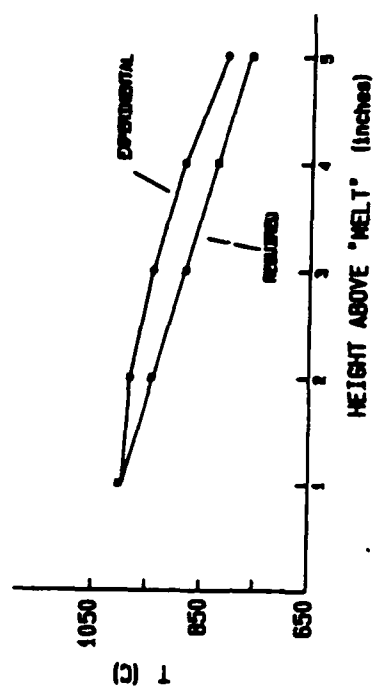
Fig. 1.7   Schematic of the original version of HFCS.

EXPERIMENTAL RESULTS USING A MODEL
CRYSTAL

MODELLING RESULTS

Fig. 1.8   Modelling and experimental results using model crystals indicate that heat transfer at the crystal periphery is not unidirectional.

carbon-graphite (to cover a spectrum of thermal conductivities) model crystals. The axial temperature distributions in the model crystals were measured by thermocouples. Several configurations simulating the presence of an opaque encapsulant, melt height, and position of the crucible in the heater cavity were considered. Results indicated that for the majority of configurations the crystal was heated by the crucible [2]. These observations led to the redesign of the HTCS to provide for control of heat transfer into, as well as out of, the crystal. In the modified HTCS a cold plate was installed around a redesigned version of the heater assembly, thus effectively isolating the HTCS from the hot crucible walls. The capability to control the temperature field in the crystal by adjusting the heater power levels in the five zones of the HTCS was explored numerically using a simulation package developed for this effort. An algorithm for controlling heat transfer from the crystal based on thermocouple readings was also developed. Simulation results established that by adjusting the radial and axial temperature variations in the HTCS, through modulation of heater powers at precalculated levels, the radial temperature gradients in the crystal can be eliminated.

The modified HTCS was installed in a growth furnace and tests using graphite model crystals were performed. The tests results and a schematic of the installed HTCS are given in Fig. 1.9. With the HTCS heaters inactive, the axial temperature distribution of the crystal exhibits that of a system subject to radiative cooling. With the HTCS heaters controlled according to the previously developed algorithm, radial

- 35 -

Growth Simulation Using Carbon Graphite Crystal to Quantify the Effect of the HFCS
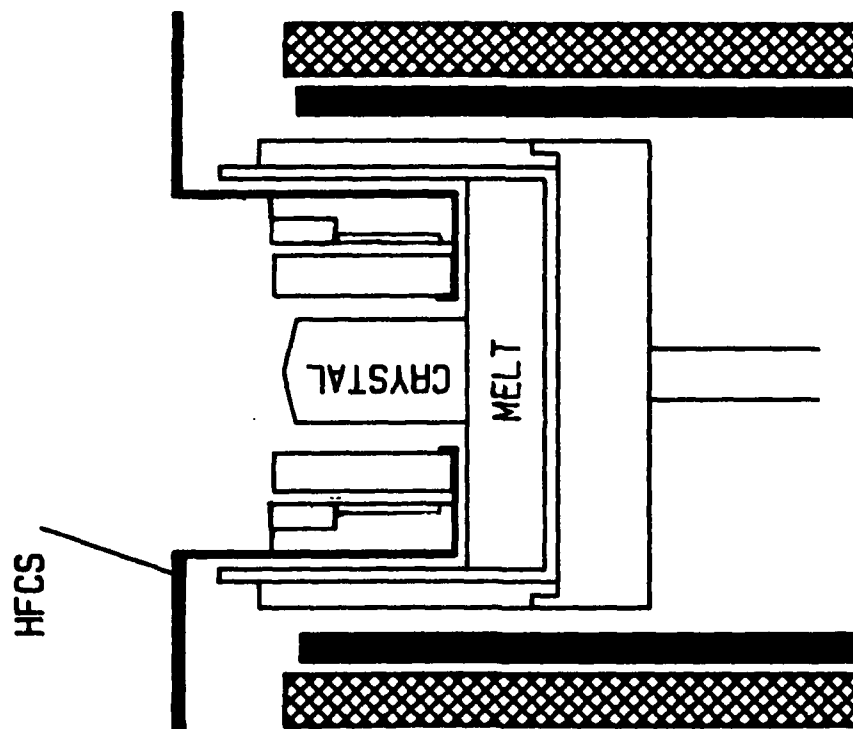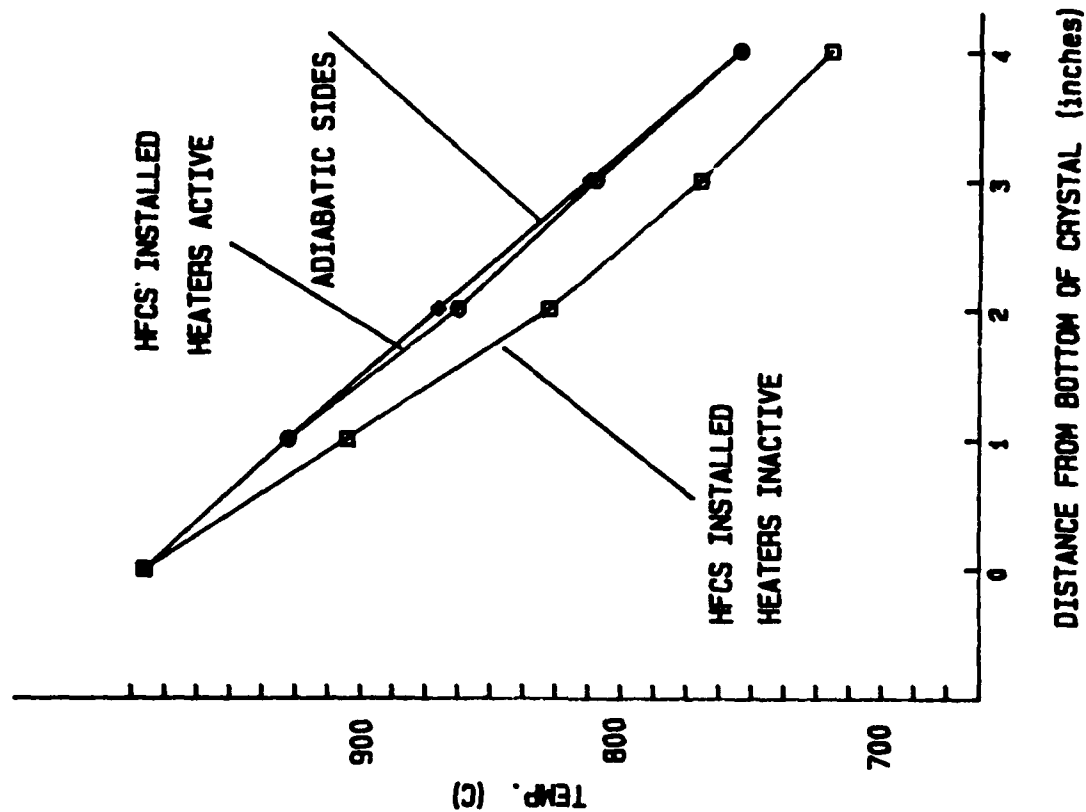

Fig. 1.9   Schematic of the modified HFCS installed in the growth system, and the results of experiments corroborating its ability to create a linearly decreasing temperature profile (eliminating radial temperature gradients) in the model crystal.

temperature gradients in the crystal were eliminated and a nearly axial temperature profile in the model crystal was obtained.

The ability of the HTCS to both withstand the elevated temperatures and function as predicted in controlling heat transfer from the crystals suggests that it is ready to be used in growth experiments. Presently a LP–LEC system is being refurbished for installation of the HTCS and growth of GaAs. Growth experiment results should become available in summer 1988.

References

1. A.S. Jordan, R. Caruso, and A.R. Von Neida, Bell Syst. Tech. J. 59 593 (1980).

2. K.W. Kelly, M.S. Thesis, Department of Mechanical Engineering, MIT, 1987.

2. MAGNETO-HYDRODYNAMICS

MATHEMATICAL MODELLING OF FORCED FLOW IN MAGNETICALLY DAMPED MELTS

The purpose of this investigation has been to obtain an improved insight into the behavior of magnetically damped Czochralski systems from the standpoint of fluid flow, heat flow, and dopant (impurity) distribution.

In the first instance we considered an idealized case of a crystal of infinite radius immersed in an infinite melt; under these conditions it was possible to obtain relatively simple numerical solutions and analytical asymptotes [1]. This work has provided us with both an excellent appreciation regarding the interdependence of the key process parameters and, equally important, with a basis for testing the subsequent numerical solutions.

More specifically, the role of the magnetic interaction parameter was defined and the significant damping of convection by a magnetic field will occur when this magnetic interaction parameter exceeds unity.

This work was subsequently extended to consider the partitioning of a dopant between the crystal and the melt from which it is being grown [2]. We found that both the magnetic field and the growth rate of the crystal can play an extremely important role in affecting the partition coefficient. The specific semi-analytical relationship that could be developed for the partition coefficient clearly showed the power of this asymptotic approach.

Having obtained a broad brush definition of the system, in terms of semi-analytical asymptotic solutions, we initiated the development of numerical solutions to the problem [3].

We considered an axisymmetric system and simultaneously solved Maxwell's equations, the Navier-Stokes equations, the differential thermal energy balance equation, and the mass transfer equation for the dopant distribution. Perhaps most important, the numerical solutions did indeed approach the analytical asymptotes in special cases. This provided a means for calibrating the numerical approach.

The important results obtained from the numerical solution of the governing equations were the following:

1. A magnetic field, corresponding to a magnetic interaction parameter of larger than unity (in the kGauss range for typical Czochralski systems) does indeed suppress convection.

2. The extent to which convection is being suppressed reduces the convective heat transfer component, so that most of the energy transported within the melt is by condition. This will allow rather more ready control.

3. Since the Schmidt number is much larger than the Prandtl number, magnetic fields in the kGauss range do not suppress convective mass transfer. Indeed, unless extremely large fields are being provided (20-30 kGauss), mass transfer will occur primarily by convection.

4. Preliminary calculations show that by using fields in the range of 20–40 kGauss convection would be totally suppressed and the dopant would be transported to the crystal by diffusion only.

References

1.   R.A. Cartwright, N. El-Kaddah, and J. Szekely, "The Effect of an Axial Magnetic Field at the Interface of a Crystal Grown by the Czochralski Method," IMA J. Appl. Math. 35, 175 (1985).

2.   O.J. Ilegbusi, J. Szekely, and R.A. Cartworght, "Some Asymptotic and Computed Results on Magnetically Damped Czochralski Crystal Growing Systems," J. Physicochemical Hydrodynamics 10 (1) 33–51 (1988).

3.   R.A. Cartwright, D.T.J. Hurle, R.W. Series, and J. Szekely, "The Influence of Crucible Rotation on the Effective Distribution Coefficient in Magnetic Czochralski Growth," J. Crystal Growth (1987).

3. CONTROL THEORY

ADVANCED CONTROL DESIGN

The traditional approach to control system design for the Czochralski process has been the establishment of constant crystal diameter. However, the actions taken by automatic diameter control systems simultaneously influence the properties of electronic materials due to the coupled nature of the process physics (e.g. heat, mass and momentum transfer). Since advanced device processing requires precise control of many of these parameters, we found it necessary to define and implement a richer set of control objectives. It is therefore considered important that the effects of all the available system inputs (e.g. rotation rates, lifting and pulling rates, heater parameters, etc.) be weighed when controlling the growth process.

Conventional control systems for the Czochralski process use a combination of empirically derived feedforward input trajectories (predetermined process changes without feedback) and closed loop regulators such as the selection of (1) crystal and crucible rotation rates to modify dopant segregation behavior, and (2) heater and pulling rate trajectories to obtain desired crystal shape and seeding conditions (necking) which are expected to reduce grown-in dislocations. Even though closed loop diameter control (ADC) can be implemented with a variety of different inputs and outputs [1], it is generally characterized by a single-input-single-output (SISO) control structure. In some cases, though, a constraint is applied that keeps the pull rate within a specified bound.

The limitation of the conventional Czochralski control system design approach is that the process–materials properties interactions have not been explicitly incorporated as part of the control design process. We found that conventional control system designs do not explicitly address important process dynamics, particularly the time variation of the process and batch related disturbances.

The material requirements and related process phenomena considered in the present design study are listed in Table 1. To account for the cross coupling between the informal objectives and the process phenomena, a trade–off analysis must be made to determine the operating regime. The regime is specified in terms of the control objectives listed in Table 2. The control objectives are related to a specification of output variable set points or trajectories that the control system is designed to maintain throughout the batch cycle. The main difference from the conventional approach is that a broader set of control objectives is used.

Control Principles

There are two basic control types: open and closed loop. Open loop, or feedforward control, uses either an empirical or model derived input signal, u_{req}, to drive the plant, $g(s)$. The performance, however, is limited since there is no compensation for errors. Feedback structures (Fig. 3.1) use a measurement of the system output, $y(s)$, to develop a corrective input signal by the controller, $k(s)$, that compensates for errors. Corrective action, however, is taken only after an error has

TABLE 1: INFORMAL CONTROL OBJECTIVES

Informal Objectives	Related Process Phenomenon
Segregation	
Dopant distribution	Fluid flow
Contaminant distribution	–Near field flow
(Stoichiometry) *	–Buil stability
	Melt thermal symmetry
	Interface shape
	Growth rate variation
Defects	
Dislocation	Crystal thermal gradients/
–Thermal stress	crystal heat flux
–Grown–in	Interface shape
(EL2) *	Crystal shape (necking)
(Vacancies) *	
(Stoichiometry) *	
Bulk Shape	
	Crystal diameter

*Not considered in this level of design.

TABLE 2: FORMAL CONTROL OBJECTIVES

Maintain interface shape

Maintain crystal heat fluxes

Maintain melt thermal–fluid characteristics

–Bulk flow stability (turbulance/3D flow)

–Thermal symmetry

–Melt gradient to prevent supercooling

–Required near interface flow characteristics
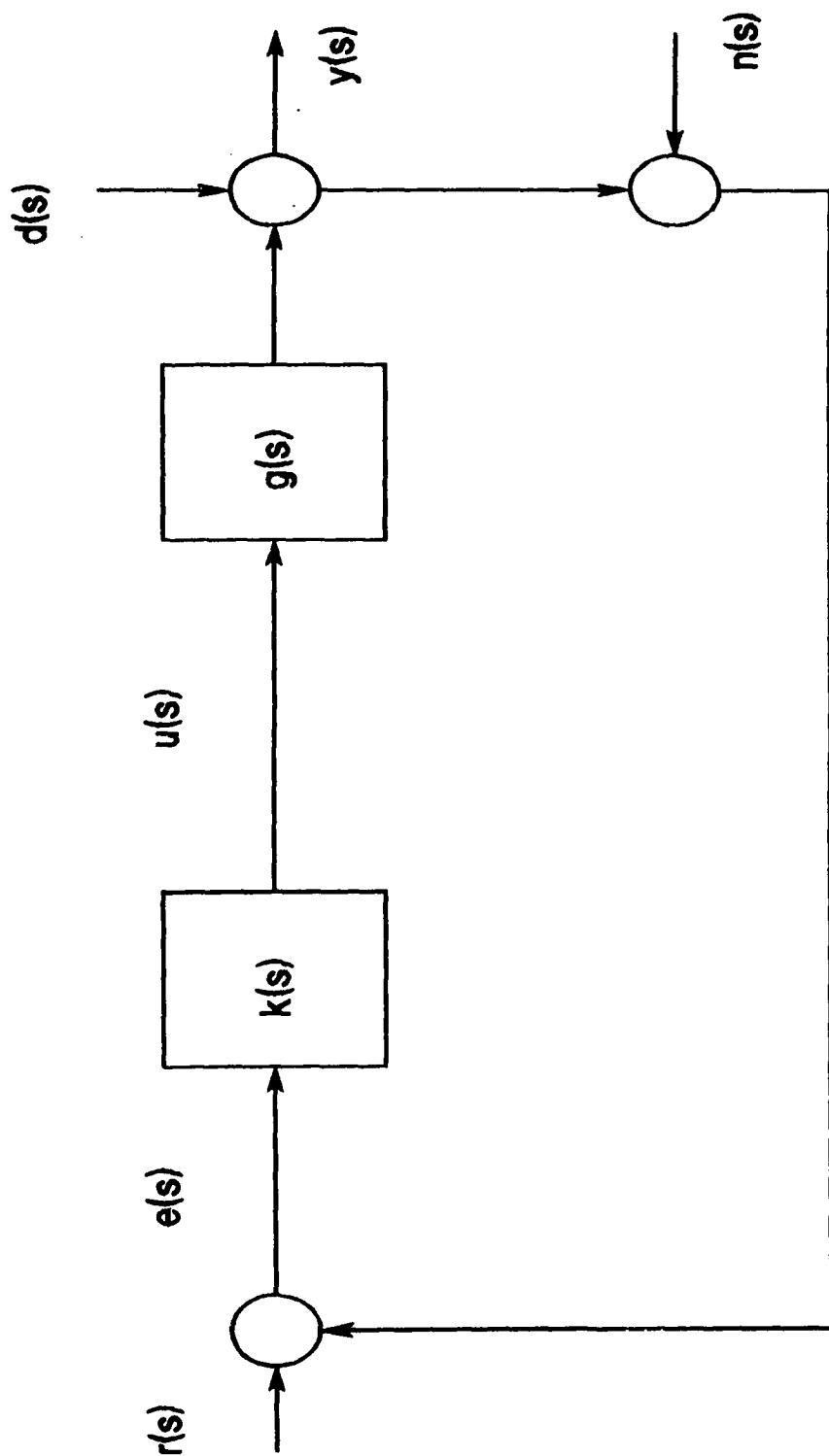
Growth rate variation constraint

Fig. 3.1 Conventional feedback structure.

occurred. The presently developed model-based control (MBC) incorporates both aspects, using a model to determine the control input as it is needed and feedback to compensate for the model errors.

The closed loop control structure design entails choosing the control variables that achieve the best controller performance [2]. The features that the controller should be able to achieve are (a) reject disturbances, $d_o(s)$, (b) follow the command signal, $r(s)$, (c) correct for modelling errors, $\Delta m(s)$, and (d) be insensitive to noise, $n(s)$, that corrupts the measurements.

Control theory reveals a number of important insights into the Czochralski system that should be considered in the design process. The important points include:

(1) frequencies over which good disturbance rejection and command following is achieved must be lower than the noise spectrum;

(2) high control gain results in good control, but the usable control gain is limited due to instability that can be caused by feedback over frequencies where model error is large;

(3) performance is limited if $g(s)$ has a right half plane (RHP) zero [2,3] since the RHP zero must be excluded from being used in the control law, becoming an unstable pole when inverted;

(4) small gain systems, where $|g(s)|$ and the frequency, ω_c, at which roll-off occurs are small, pose difficulties to achieving good controller performance (particularly for disturbance rejection) due to robustness limitations.

System and Disturbance Dynamics

The process and disturbance dynamics are revealed by a low order model (LOM) of the process. Heat flows from the heater to the crucible and into the melt. In a conventional system, the heater/crucible system is coupled to the crystal since the crystal is exposed to more of the hot crucible wall. As the crystal grows longer, it is exposed to a changing thermal environment and, thus, the heat flux leaving the crystal, Q_x, varies with time.

The melt depletion also causes time variation of the thermal melt mass and the heat transfer since the crucible and melt contact area and geometric relations change. The result is that the heater/melt system's eigenstructure is time-varying. The melt and crystal heat fluxes are time-varying and therefore act as disturbances.

A variety of diameter related measurements can be made. Experimental identification by Hurle et al [4] and analysis of the measurement equations shows that the weight measurement has a RHP zero. As discussed, this poses a fundamental limitation on controller performance. The severity of its effects depends on the operating regime which determines the relative pole/zero location. In general, the

performance is affected more as the RHP zero becomes slower. The RHP zero also reduces the ability to estimate other quantities such as R_i and ϕ.

The meniscus angle, ϕ, relates how the radius, R_i, is changing, as pointed out by Hurle [1]. Direct measurement of ϕ is preferred to differentiating the diameter output since differentiation amplifies the noise present (also true for differentiating the weight signal).

The dynamics of the inputs and the outputs are represented by the plant frequency response (i.e. the Bode plot), shown in Fig. 3.2. The important characteristics include the fact that the bandwidth of the pull rate, V_p, input (curves b,d) is greater than the heater input, P_{in}, (curves a,c). The heater input is slowed down by the heater, crucible, and melt thermal capacitances and resistances, while V_p has a more direct affect on the interface.

The output curves reveal that the bandwidth of ϕ (curves c,d) is greater than those related to R_i (curves a,b). However, the steady state value (i.e. $\omega=0$) of ϕ is zero since $R_i=0$ in steady state. ϕ, therefore, must be used with a measurement of R_i. ϕ should be explicitly measured or estimated so that its feedback gain level can be independently set. The choice between different estimation methods should be based on the noise and steady state sensitivities.

The Bode plot shows that the bulk interface dynamics are slow, with roll–off beginning around 0.001 radians/second. As such, it is important to compensate for
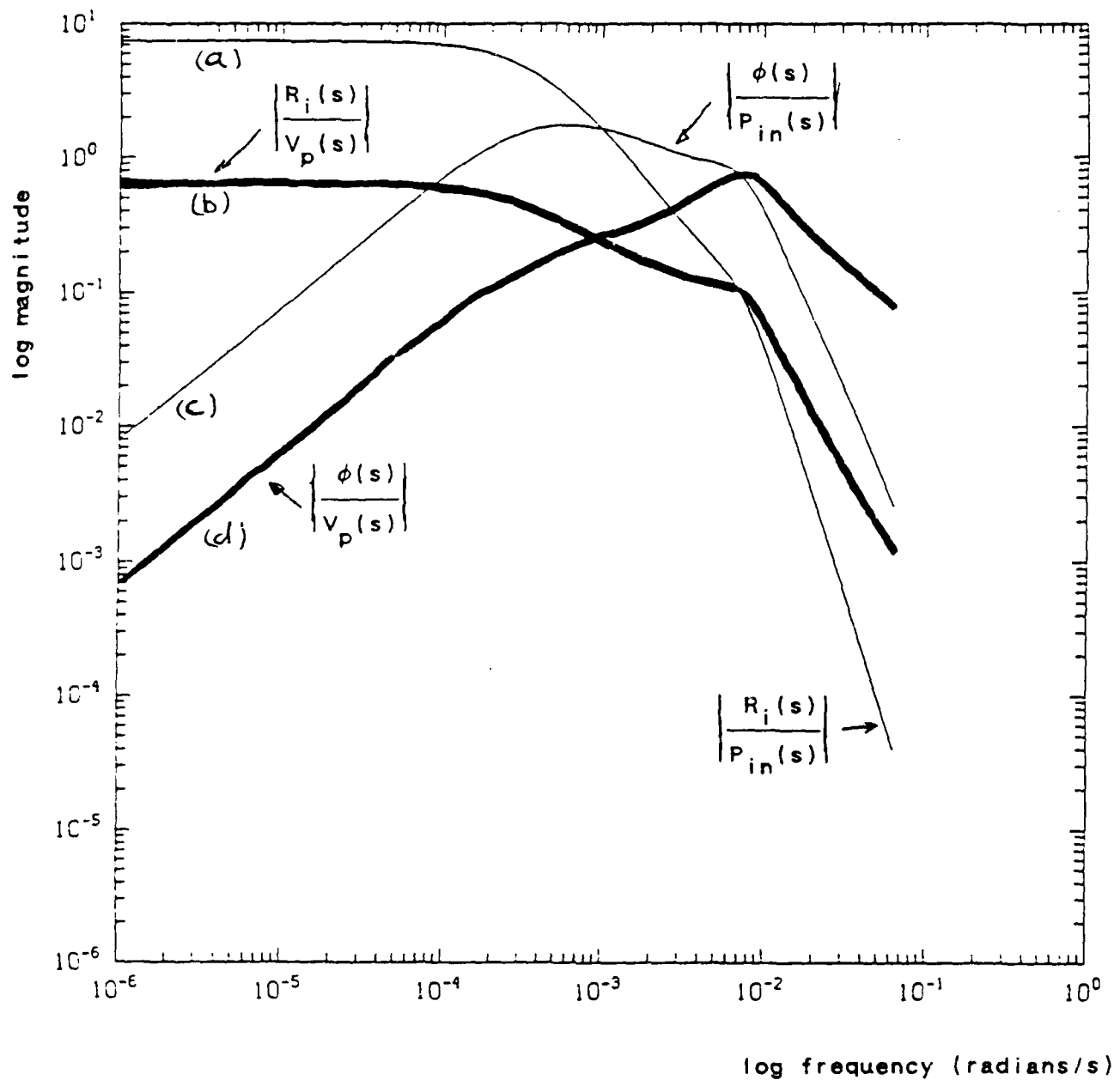
Fig. 3.2   Bode plots of normalized open loop plant transfer function; curves:
(a) radius output to heater input; (b) radius output to pull rate input;
(c) meniscus angle output to heater input; (d) meniscus angle output
to pull rate input.

the melt's heat flux disturbances and changing eigenstructure before a radius error is created.

Control Structure Design

The proposed general control structure is described in Table 3. Variables that cannot be measured are controlled by a feedforward structure. The trajectories employed can be derived from both experimental and modelling analysis. Local feedback loops are employed to maintain the input trajectories.

A closed loop regulator maintains the interface growth dynamics while meeting the melt and crystal thermal requirements. As a first step, the control structure is

TABLE 3: GENERAL CONTROL STRUCTURE

Feedforward Control

Objectives	Feedforward Trajectories
Segregation –Bulk melt stability –Near field fluid flow Thermal Dislocation Formation	Crucible rotation Seed rotation Magnetic field Interface shape Crystal heat flux

Closed Loop Regulator (MBC)

Interface
–Diameter
–Shape
Crystal heat flux
Melt thermal distribution
–Bulk temperature
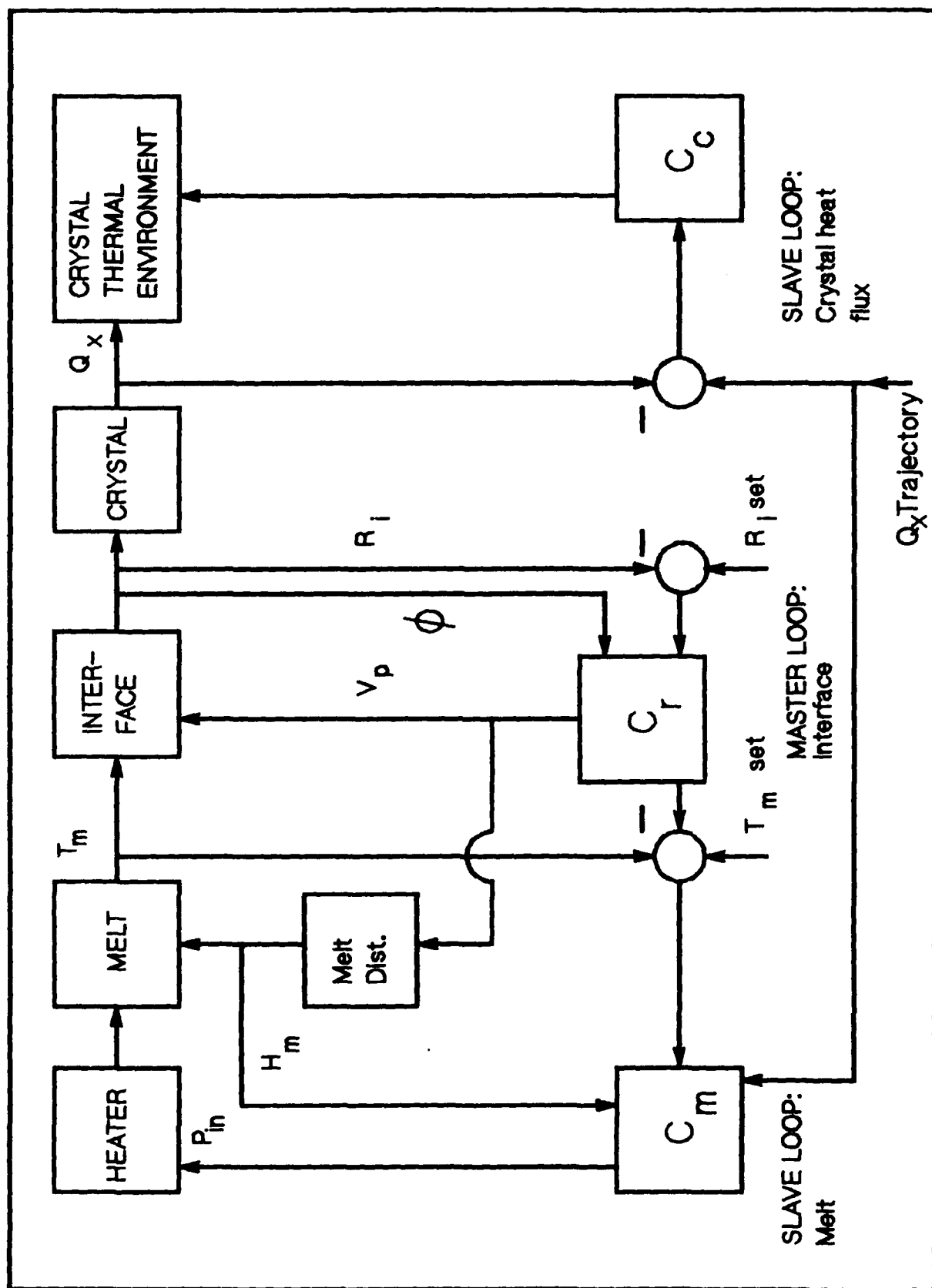–Temperature gradients
–Symmetry

designed to compensate for the batch disturbances and time-varying eigenstructure. The regulator, depicted in Fig. 3.3, consists of a master loop around the interface and slave loops around the melt and crystal [5]. A model-based control law is used to compensate for the melt's time variation and disturbances (Fig. 3.4).

The crystal slave loop eliminates the crystal heat flux disturbance and meets the crystal heat transfer control objective related to dislocation formation. Actuators that modulate the crystal-environment heat transfer can be used, such as axially segmented heaters or a heat pipe scheme. The fast dynamics of the crystal-environment in comparison to the interface dynamics limits the cross-coupling between the two.

The interface master loop uses the R_i and ϕ outputs, partitioned into low and high frequency bands. The low frequency error determines the melt set point. The melt slave loop maintains the required heat flux from the melt to the interface, Q_i, and compensates for the melt disturbance before it affects the interface. If a crystal heat flux trajectory is followed, then it is feedforwarded to the melt loop for feedforward compensation. The melt loop can also maintain a desired Q_i/Q_x, related to the relative interface stability.

The high frequency error drives the pull rate input, extending the bandwidth of the system. Since it has a greater bandwidth than the heater-melt loop, interference between the two loops is minimized. A band pass filter can be used to reduce the
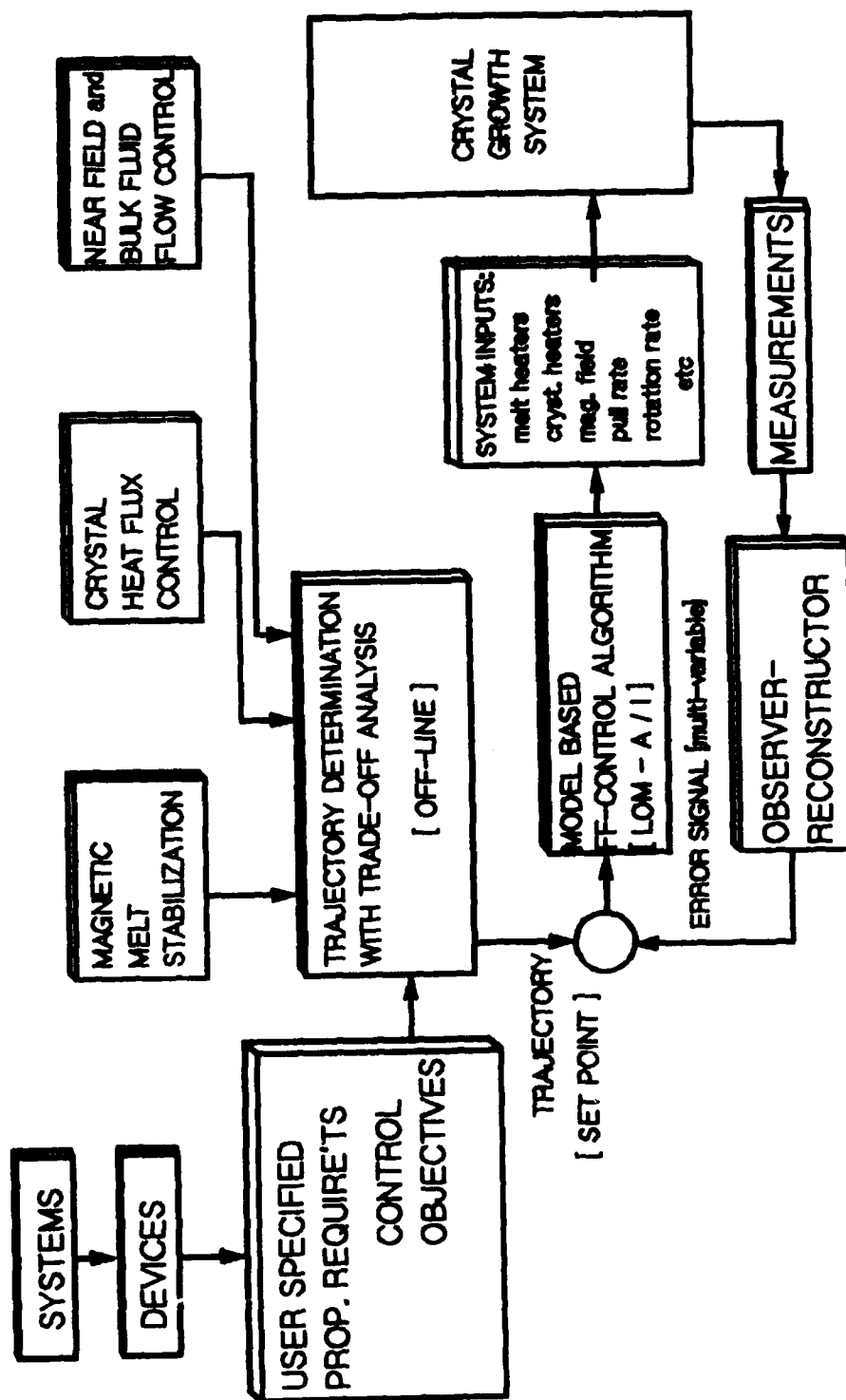
Fig. 3.3   Regulator structure.

Fig. 3.4 Model based growth control concept.

cross-coupling with the crystal heat flux slave loop and can be tuned to minimize

growth variations that may adversely affect segregation. Saturation limits for the pull

rate input can also be incorporated to minimize adverse growth/segregation variations.

References

1. D.T.J. Hurle, J. Crystal Growth 42 (1977) 473.

2. J.C. Doyle and G. Stein, IEEE Trans. Auto. Cont. AC-26, 1 Feb. (1981) 4.

3. C.E. Garcia and M. Morari, I&EC Proc. Des. Dev. 21 (1982) 308.

4. D.T.J. Hurle et al., J. Crystal Growth 74 (1986) 480.

5. Patents pending, MIT case numbers 4408 and 4447.

4. LP-LEC GROWTH

<u>THERMAL IMAGING</u>

Crystal growth using the liquid encapsulated Czochralski (LEC) technique requires precise control of the thermal field within the melt and growing crystal. The spatial temperature distribution in the melt is established by the hot zone, crystal, and environmental thermal boundary conditions. In conventional growth systems, a single–input–single–output (SISO) closed loop proportional, integral and derivative (PID) controller is used to maintain and/or change a single temperature to accomplish the task of controlling the temperature distribution in the melt. Thermocouples or single color pyrometers are generally used as sensors for this purpose. The placement of the sensor is determined empirically.

The non–axisymmetric nature of the melt surface temperature distribution causes periodic fluctuations in the microscopic rate of growth during rotational pulling. Turbulent convection, present in the LP–LEC melt due to unavoidable radial and axial temperature gradients, is found to generate random melt temperature fluctuations which reappear as chaotic variations in dopant concentration superimposed on the periodic rotational variations discussed above. Application of magnetic fields to the melt eliminates melt turbulence and its related effects on growth and segregation. It has also been observed to change the magnitude of radial temperature gradients in the melt. Since this gradient controls to a major extent the sensitivity of the crystal

- 54 -

diameter to overall changes in hot zone temperature, the quantitative evaluation of the melt surface thermal field was considered critical to the development of an improved growth control scheme. To this end, a real-time thermal imaging system has been developed.

Thermal field measurements made in the presence of magnetic fields with a Vidicon, or "tube," camera proved unacceptable due to the interaction with the magnetic field. Thus, a solid-state charge coupled device (CCD) camera design was chosen. The peak of the black body radiation for the GaAs/melt system is in the infrared; optical measurements of boric oxide indicate transparency in the visible and absorption of the IR spectrum by this encapsulant. These findings led to the selection of a 1-nm bandpass at 632 nm for thermal imaging. This wavelength is near the steepest region of the black body curve, which ensures a large intensity change for a given temperature change; sensitivity is high.

Hardware Configuration and System Architecture

The high termperature scene is viewed in near normal incidence by a low noise (-60 dB) charge coupled device (CCD) camera (RCA, 512 by 512 pixels). In this way, an array of 1/4 million discrete optical pyrometers is available to characterize the scene with a spatial resolution of better than 0.5 mm. A narrow band pass filter (1 nm, centered at 633 nm) is used to obtain a monochromatic image at a wavelength which matches the peak in the spectral sensitivity of the CCD element

while maintaining a steep slope on the Intensity vs. Temperature curve of the emitting surface.

The major components of the imager (Fig. 4.1) include the CCD camera and narrow bandpass filter, the image processing subsystems (Recognition Technology, Inc.) with high resolution analog RGB monitor and the host computer with integral high speed data acquisition and control capability (Masscomp MC-5500).

The camera provides 30 frames/second using a standard RS-170 configuration. Adjustment of gain and dc offset of the CCD camera's output is accomplished by an A/D subsystem which permits operation at high gain for maximum sensitivity. The signal is preprocessed with user defineable look-up tables (LUT) to correct for inherent nonlinearities within the camera and is digitized to 8 bits (256 gray levels). Image processing functions are carried out in the pipelined pixel processor. Other principle tasks include image storage and transfer within the digital storage units. A unique capability of the system is the dual ported nature of the digital storage units. Image memory appears as extended system memory on the host; thus, image data can be accessed simultaneously by the pipelined pixel processor and the host CPU. Parallel processing of the information can be accomplished with no performance penalty. Real-time graphics overlays and linear convolutions are produced in this manner. Two of the digital storage units are configured as a 16-bit pair to hold high precision intermediate results produced during
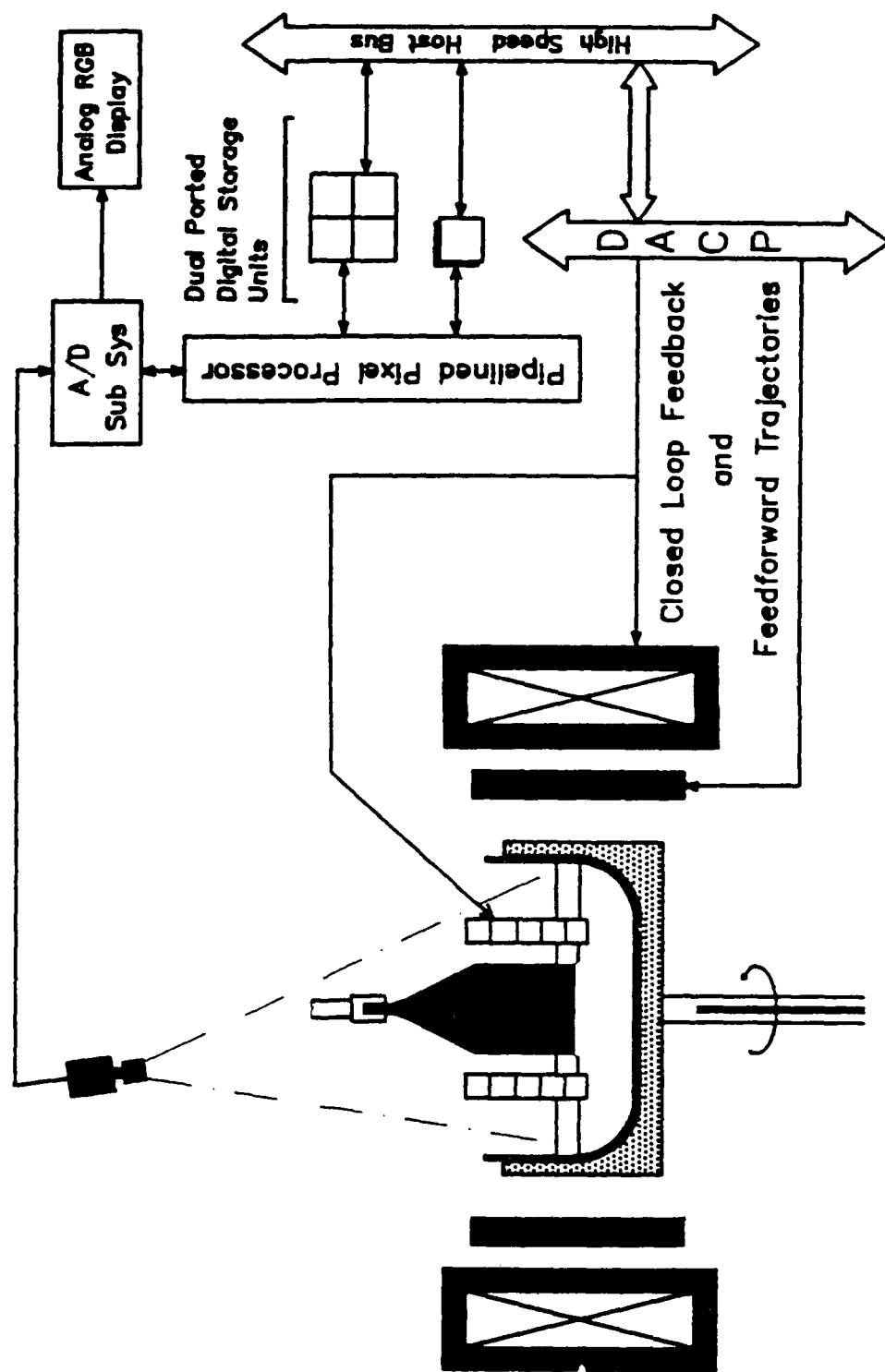
Fig. 4.1   Thermal imaging architecture and preliminary control structure for LEC growth of GaAs.

certain image processing calculations (e.g. 2-d convolutions and temporal averaging). A third 1024 by 1024 image memory unit is configured as four contiguous 512 by 512 frame stores.

The processed images (in real time) are sent back through the A/D subsystem where a second LUT is used to false color the outgoing monochrome signal. The LUT is defined to map low intensities to blue and high intensities to red, with a linear interpolation of the complete 8-bit dynamic range. The complete spectrum between blue and red corresponds to intensities from 0 to 255 gray levels. The output is displayed (with graphics overlays) on the high resolution RGB monitor.

Thermal information is selectively extracted from the thermal image and passed, via the host, to the Data Acquisition and Control Processor (DACP). The raw thermal data is scaled and offset to conform to the required output characteristics (e.g. a platinum/platinum-10% rhodium thermocouple) and sent from a digital to analog (D/A) converter to the crystal puller to be used for temperature control.

Thermal Imaging of Encapsulated Melts

The CCD camera is, by necessity, mounted off-axis and non-normal to the crucible. The crystal pull shaft is on the rotational axis and the camera axis is located 3.5 inches from it, inclined at 5° to the normal. As a result, internal reflections from the melt surface are reduced but not totally eliminated. The high

temperature scene comprises the melt, crucible, heater elements, crystal, and pull shaft. However, the only portion of the scene which provides optical information that is readily convertible to temperature is that emitted from the melt.

A spatially and temporally averaged thermal image of an unseeded GaAs melt viewed through the B_2O_3 layer is shown in Fig. 4.2. False color representation of the high temperature scene depicts high melt temperatures as red and lower temperatures as progressively bluer. The horizontal line crossing the encapsulated melt represents a linear array of picture elements (pixels) from which temperature data is extracted, processed, and displayed in real time (curved line above the displayed horizontal pixel array). The data has been processed by a linear convolution to remove high spatial frequency components. This processing was off-loaded from the pipelined pixel processor to the main CPU to maintain real-time performance. The gray level scale on the ordinate corresponds directly to temperature. (Calibration of the gray scale is discussed below.) Thus, the slope of the line indicates the magnitude of the radial temperature gradient. In some instances gas bubbles in the encapsulant are depicted. The effect of gas bubbles in the image can mask temperature information. Continuous temporal averaging of consecutive images (with exponential de-emphasis of previous frames) can be used to illuminate the effect of these spatial perturbations. The temporal averaging facility operates in real time and the number of frames averaged is user selectable.
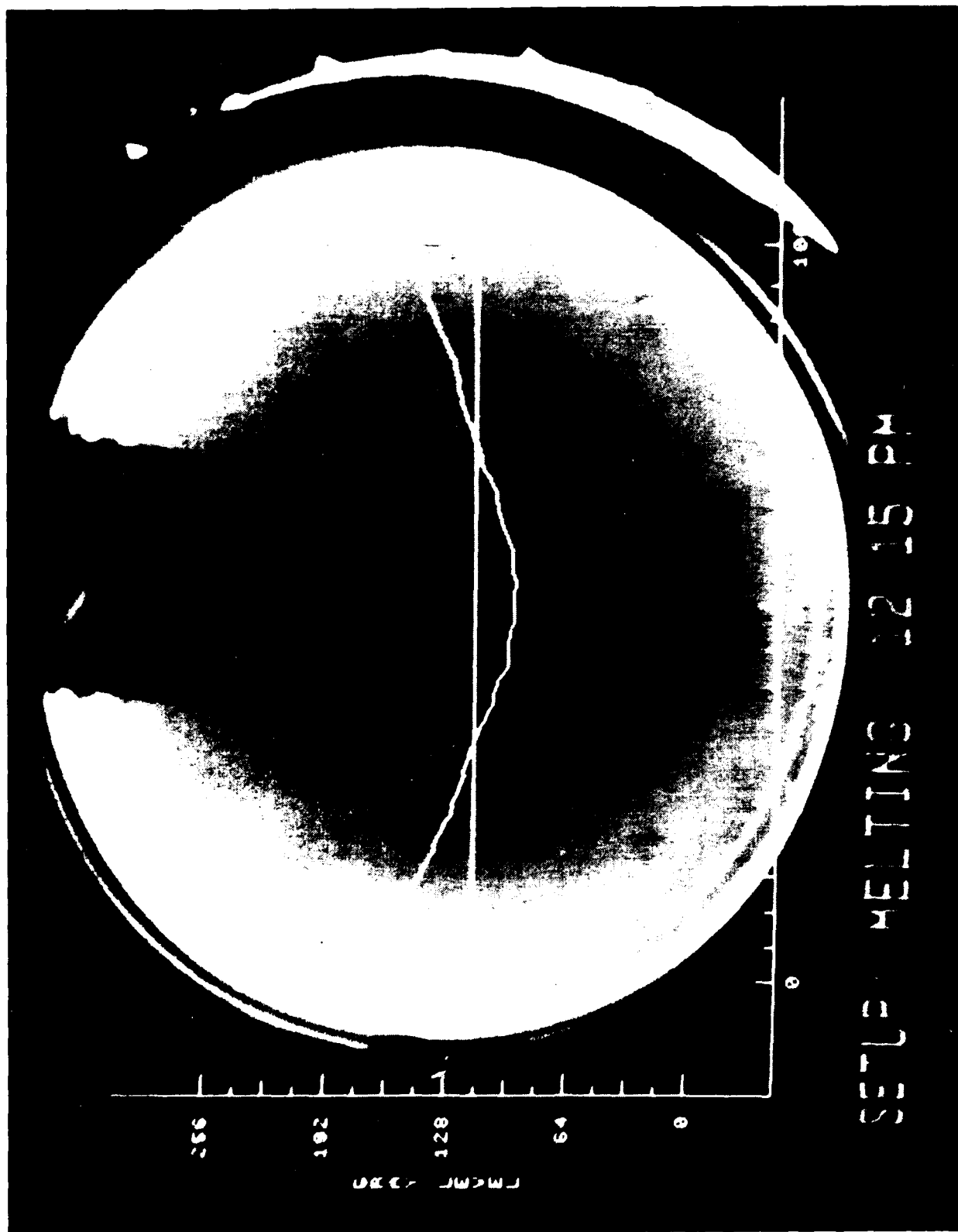
Fig. 4.2 Thermal image of an encapsulated GaAs melt. Temporal averaging has been used to eliminate the effect of gas bubbles present in the encapsulant.

A thermal image taken during the initial stages of magnetically stabilized GaAs growth (2000 gauss) is shown in Fig. 4.3. The abrupt discontinuity of the optical intensity observed on crossing the melt/crystal boundary provides information concerning the diameter of the growing crystal and is used as a feedback signal for automatic diameter control. This approach has significant advantages (see Controls section) over the differential weight measurement used in conventional LEC growth systems for ADC (automatic diameter control).

A quantitative comparison of the thermal field in the presence and absence of magnetic fields indicates an increase in radial temperature gradient of approximately a factor of two as the field is ramped from zero to 2500 gauss.

High spatial frequency noise in a thermal image can be eliminated on a full frame basis. Such a two-dimensional convolution is performed in n frame times where n is the the number of non-zero elements in the convolution kernal (typically 8 of 9 in a 3 by 3 matrix). Thus, a complete convolution is accomplished in 8 frame times or 8/30 second. Isotherms, corresponding to constant intensity contours, are revealed by highlighting selected gray levels. The convolved image exhibits a reduction in high spatial frequency noise.

The thermal imaging capabilities are characterized by a view of the scene and display of the data at a single point in time (though it may have been time averaged). Another approach, found to be useful for systems control purposes, is to acquire and

Fig. 4.3 Thermal image of an encapsulated GaAs melt taken during the initial stages of growth in the presence of an applied axial magnetic field of 2000 gauss.

display intensity (temperature) data as a continuous function of time. Figure 4.4 shows the result of a pixel averaging alogorithm which takes intensity data from a 3 by 3 array of pixels, and displays the results in real-time overlayed on the thermal image.

A Sony BVU-800 professional 3/4-inch video tape recorder provides the capability to archive all thermal imaging data. This facilitates post-growth analysis for any location in the grown crystal. Both absolute and relative time information is preserved.

Temperature Control by Thermal Imaging

Conventional temperature control schemes in LEC growth configuration are based on sensor locations which are well removed from the critical area of interest. Using the thermal imager as an advanced single point temperature sensor, it was possible to control the temperature of the growth system from a more advantageous position within the crucible. The intensity (temperature) information from the imager was rescaled (gain and d.c. offset) so that the output of the D/A converter, after processing by a 1000:1 voltage divider, corresponded directly to that of a Pt/Pt-10%Rh thermocouple. In this way, the signal could be fed to the conventional, analog PID controller which had previously been used to control a thermocouple placed near a heater element. The output of the thermocouple located within the crucible and the old control thermocouple (at the heater) were recorded. In both
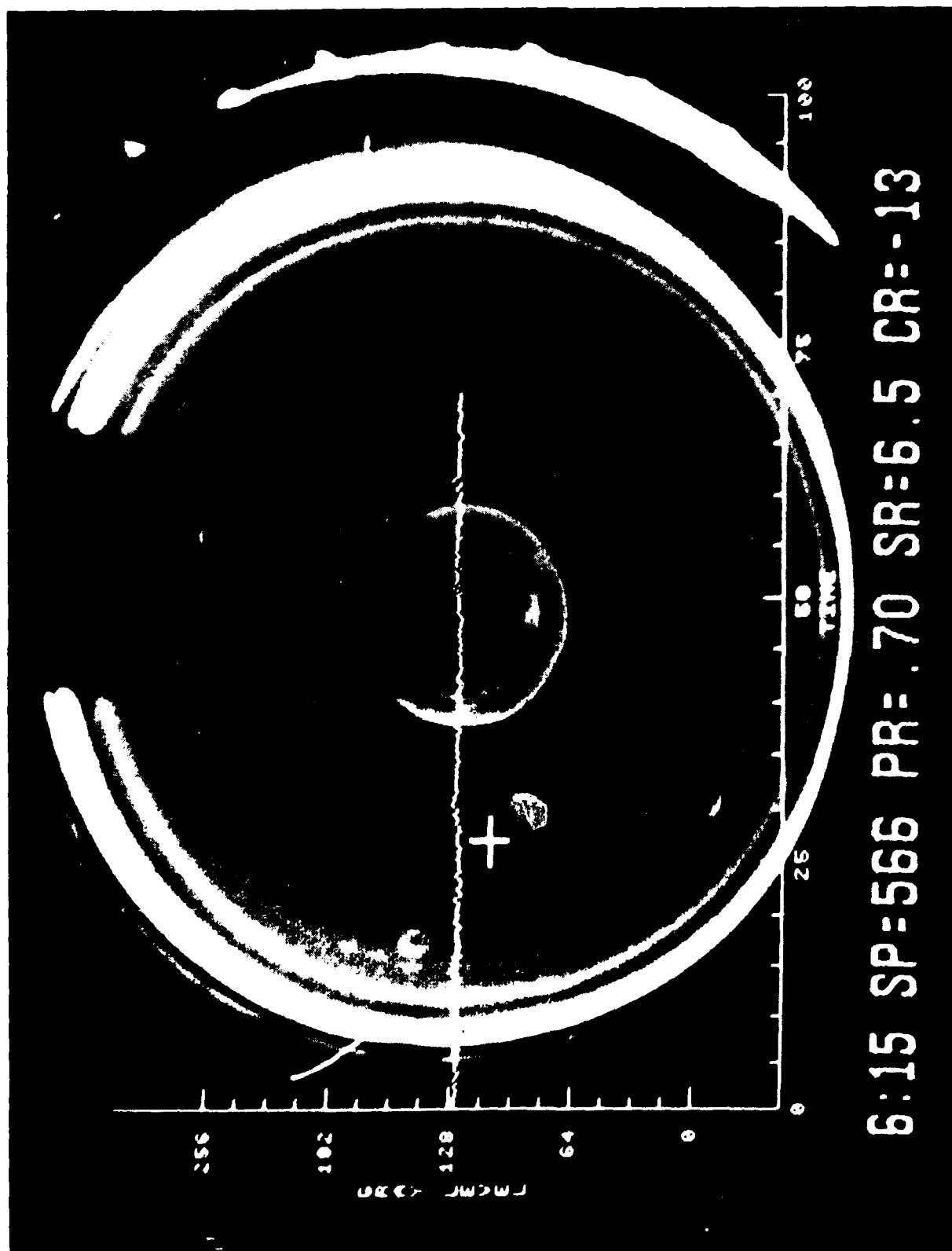
Fig. 4.4 Thermal image of an encapsulated GaAs melt with graphic display of the output of a multi-pixel averaging algorithm. The optical intensity (temperature) data is taken from a single point (defined by the cross-hair) and displayed in real time.

cases, the change in output corresponded to the temperature changes made at the controller, indicating that the signal from the thermal imager successfully tracked and measured the temperature response of the system. The ringing (decaying, oscillatory) component of the temperature response recorded by the thermocouples reflected the non-optimized PID parameters of the analog controller. These values were left unchanged from those previously determined for the thermocouple sensing the heater temperature. Considerably improved control performance is achieved with the retuning of the PID settings.

Systems Dynamics and Feedforward Control

The low pressure GaAs puller was instrumented to determine the open loop dynamics of the hot zone thermal configuration. Monitoring thermocouples were located at the heater and at the bottom of the crucible support. The thermal imager in point sensor mode (9 by 9 pixels) was used to measure the temperature near the junction of one of the thermocouples in the crucible support (Fig. 4.5). The voltage input to the power supply was linearly ramped from zero to a preselected value over the course of 1 hour. The power supply input was then held constant for 3.5 hours. During this time the power, thermocouple readings, and thermal imager output were recorded. The output of the thermal imager was translated to temperature and fitted on an absolute scale to the thermocouple data. The results for the steady power input region are presented in Fig. 4.5. With the input to the power supply held
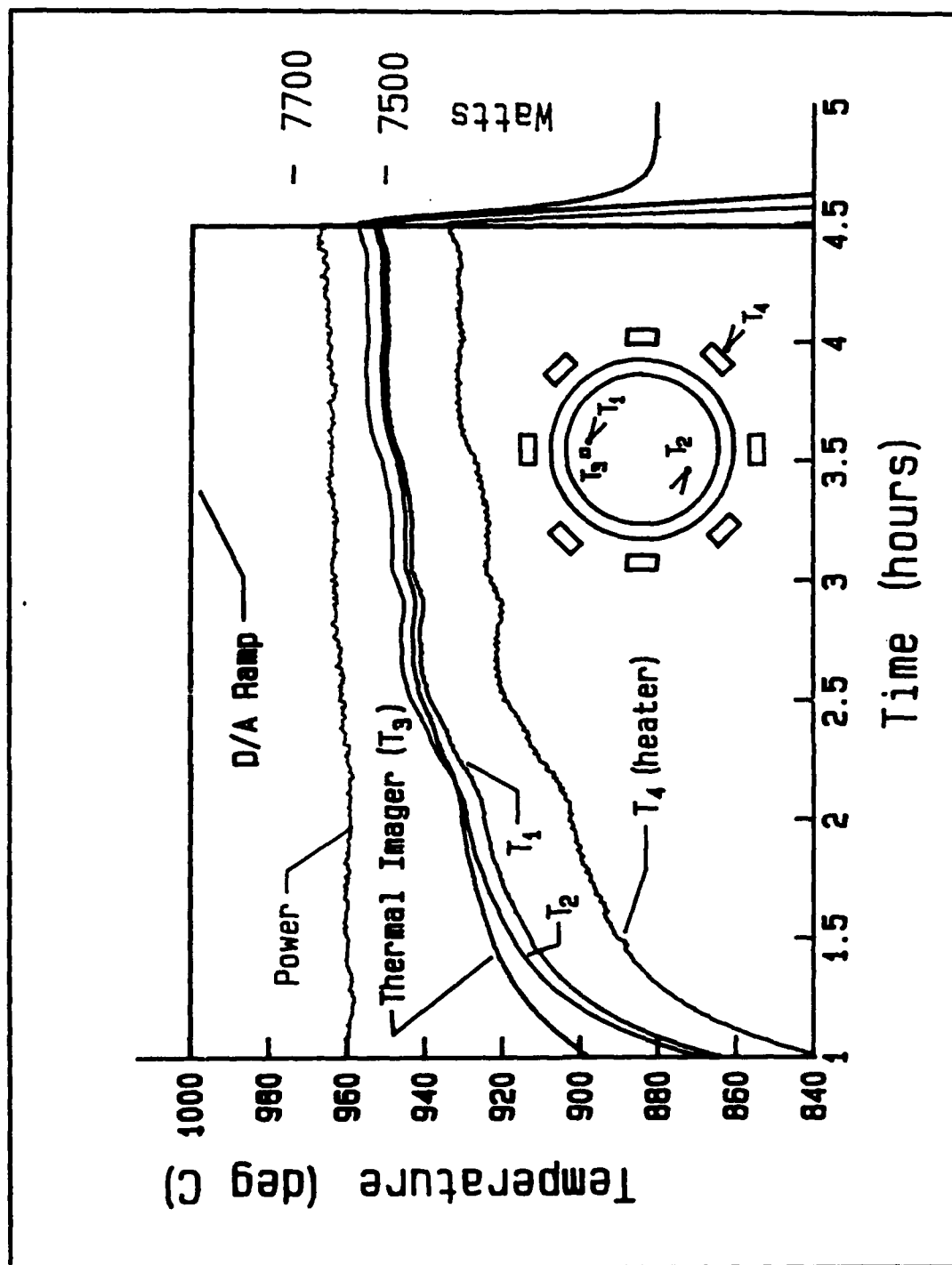
Fig. 4.5   Feedforward command following of temperature, power, and thermal imager output in response to a ramp input to the power supply of a LP–LEC puller.

constant, variations in power are detected. However, these variations are not reflected in the temperature measurements, which have a structure that is substantially different from the power response. The thermal imaging temperature data translation was obtained from the previously indicated calibration of 0.5°C per gray level. They track the thermocouple output directly. The source of the discrepancy between the power and temperature variations has not as yet been determined.

Another series of experiments was conducted to analyze the response of the system to step changes in power. Figure 4.6 shows the temperature changes that resulted. The theoretical curves were obtained from the Low Order Model (LOM) developed in conjuntion with the Systems Control program. The upper curve, describing temperature changes in the crucible, was obtained by parameter adjustment within the model to get a best fit with the experimental data. The lower theoretical curve, corresponding to the temperature changes at the heater, was predicted based on the parameters obtained in the first analysis. The close fit of the second case is indicative that the LOM captures the principle physics of the heat transfer within the hot zone.

MAGNETIC LP-LEC GROWTH OF GaAs

A standard Hamco CG-800 was modified for low pressure LEC growth of GaAs with a seed pulling mechanism (pull shaft) in place of the conventional chain lift. The gas handling system was modified to maintain up to 40 psig of argon in the
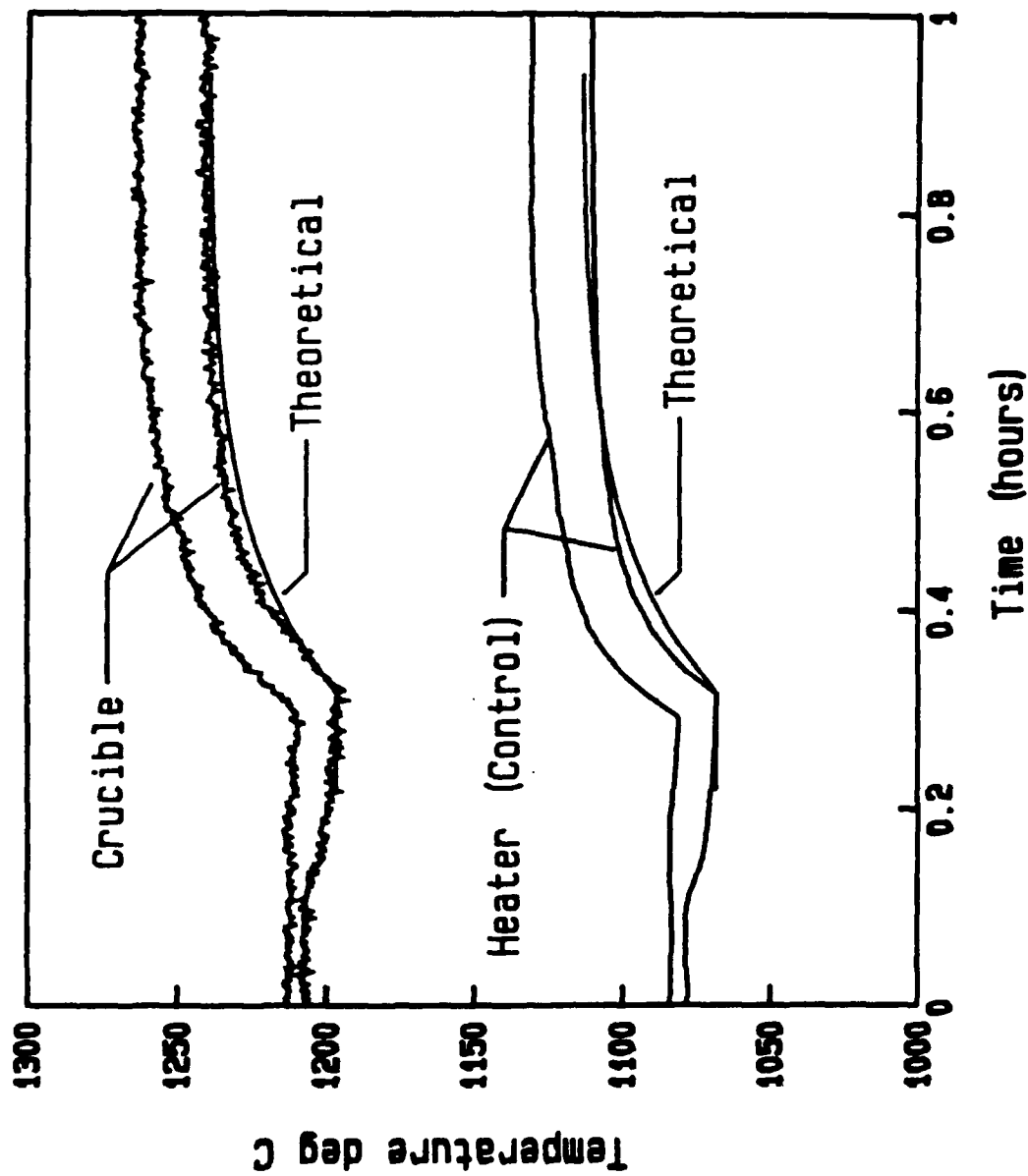
Fig. 4.6 Thermal response of hot zone to a step change in input power. Theoretical predictions are made fom the LOM description of the growth system dynamics.

chamber. A safety enclosure was constructed which surrounds the puller during operation. It is connected to an exhaust fan and ducting system which provide for continuous air flow of 1000 cfm through the enclosure.

Quantitative monitoring of the arsenic levels in the vicinity of the puller as well as on the person of the principal technician was carried out during the clean-up operation by the MIT Office of Environmental Medicine. It was found that arsenic levels were approximately 20 times lower than current OSHA standards. Protective clothing and respirators were worn by all involved personnel.

Magnetic Melt Stabilization

Growth of GaAs (charges ranging from 1 to 2 kg) without an applied magnetic field yielded crystals with an external morphology characterized by the features shown in Fig. 4.7. The "pagoda"-like shape is attributed to our inability to manually control the diameter by predictive temperature adjustments. The low radial temperature gradient in the melt associated with the hot zone configuration and crucible position is to a major extent responsible for this dynamic behavior. (For a quantitative description of the influence of the applied magnetic field on the radial temperature distribution, see the section on Thermal Imaging.)

Upon application of a 1500 gauss axial magnetic field, the dynamics of the growth process stabilize, and manual establishment of diameter by controlled temperature changes is routinely accomplished (Fig. 4.8). The stabilization is
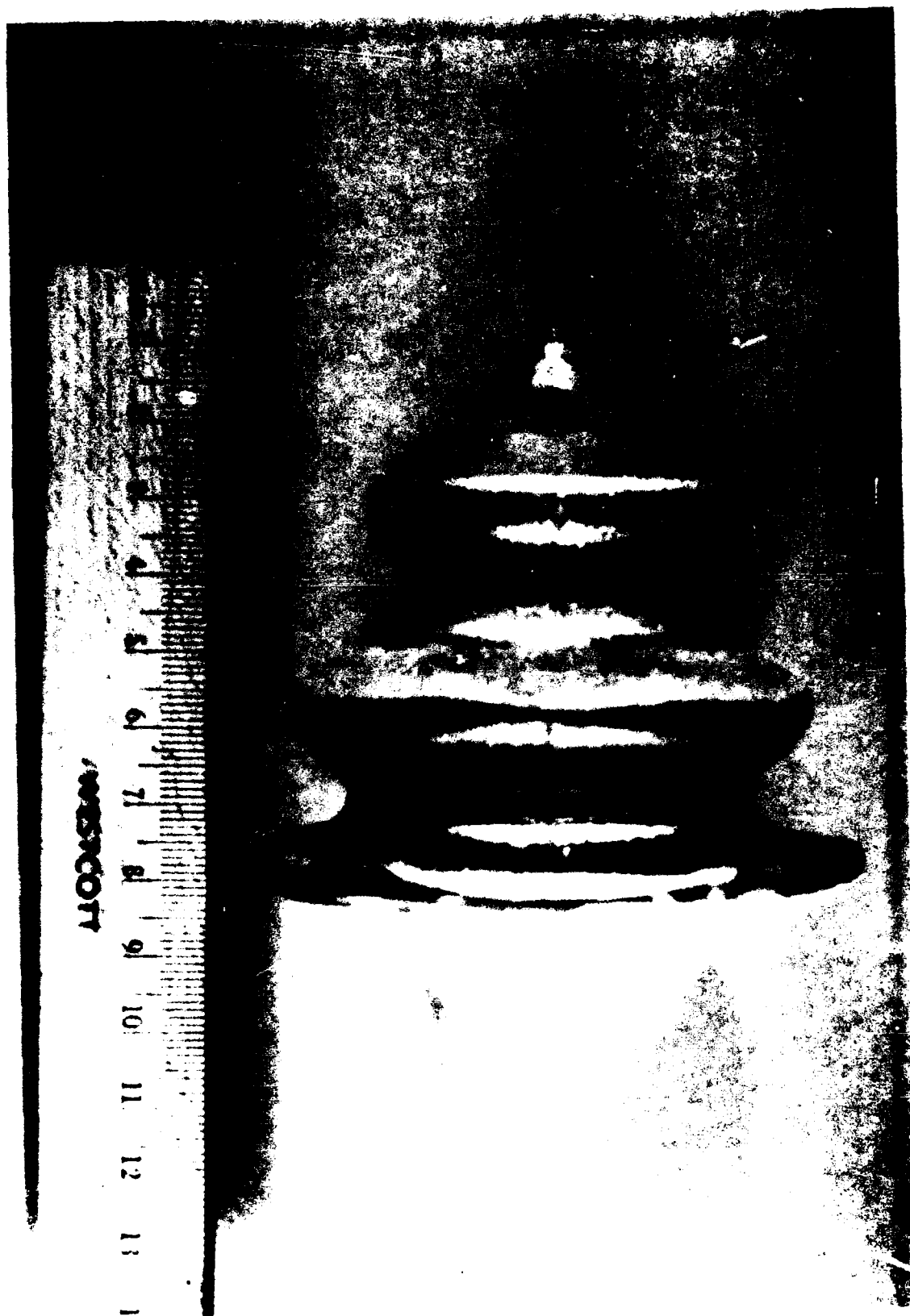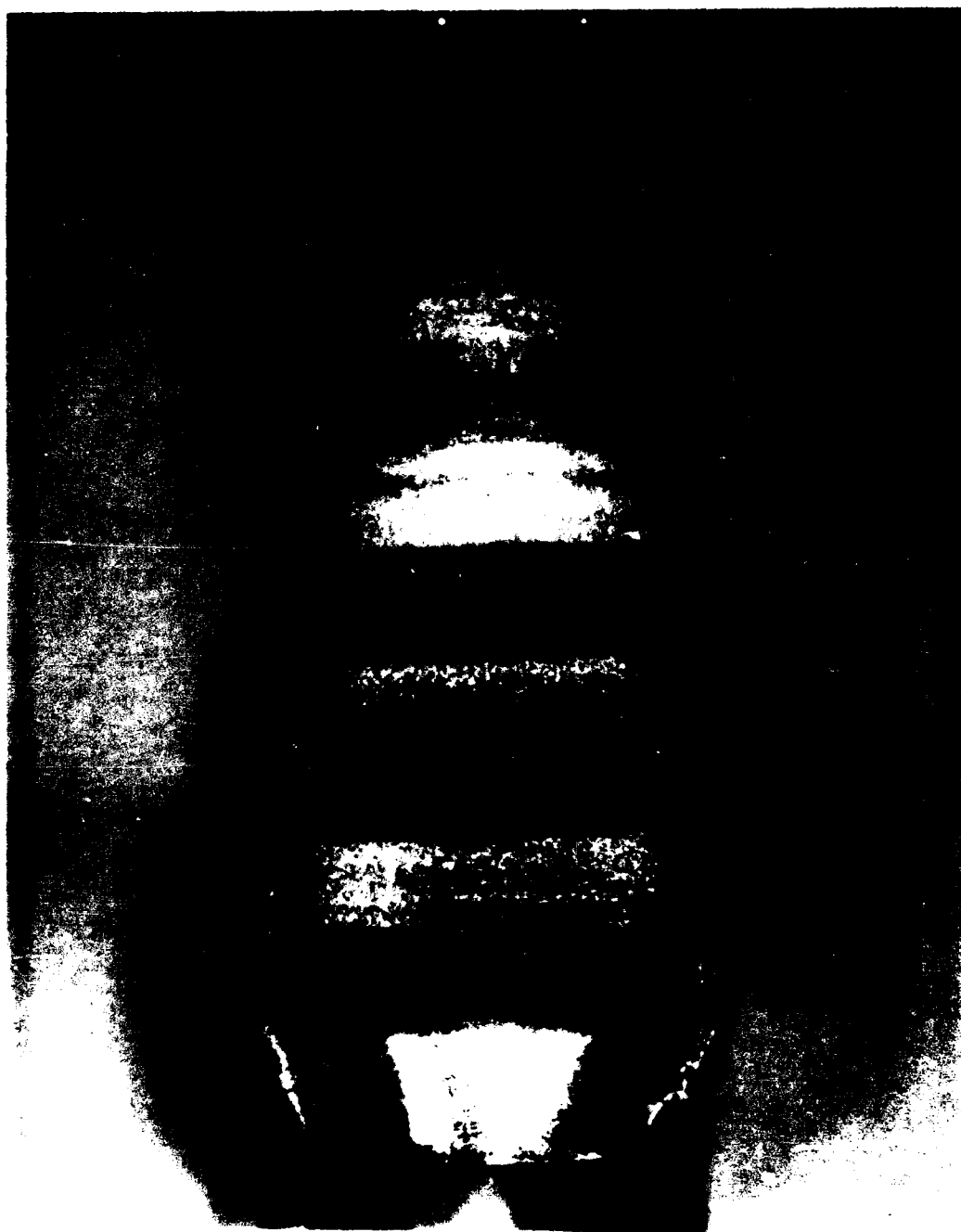
Fig. 4.7 GaAs crystal grown without magnetic field. The external morphology is indicative of our inability to manually control the diameter by predictive temperature adjustments.

GaAs 3M3-6

Fig. 4.8   GaAs crystal grown with an applied axial magnetic field of
1500 gauss. The increased radial temperature gradients in the melt
due to the field aid in stabilizing the crystal diameter.

achieved due to the increase in radial temperature gradient in the melt caused by the application of the magnetic field.

Since the magnetic field has a marked effect on the stability of the growth process, experiments were conducted to determine how the heat transfer mechanism in the melt changed in the presence of the field. For this purpose, a seed was thermally equilibrated with the encapsulated melt (as for growth) with no applied field and the set point of the temperature controller (reading a thermocouple located at the heater) recorded. The field was ramped in increments of 500 gauss from zero to 5000 gauss. After each increase in field strength, growth occurred on the seed due to the reduction in the convective component of heat transfer in the melt caused by the magnetic stabilization. After the new heat transfer conditions had equilibrated, the setpoint was readjusted to re-establish seeding conditions. The results of the experiment are shown in Fig. 4.9. Ascending from zero to 2500 gauss, the set point temperature (temperature of the heater) rose by 42°C; however, after a field of 2500 gauss is reached, no further adjustment in seeding set point was required. This indicates that conduction dominated heat transfer conditions are established in the melt at 2500 gauss. Mass transfer conditions in the melt are not influenced to the same extent since the Schmitt number of GaAs is so high compared with its Prandtl number (~10 vs. 0.05). As a result, the residual melt flows do not affect the heat
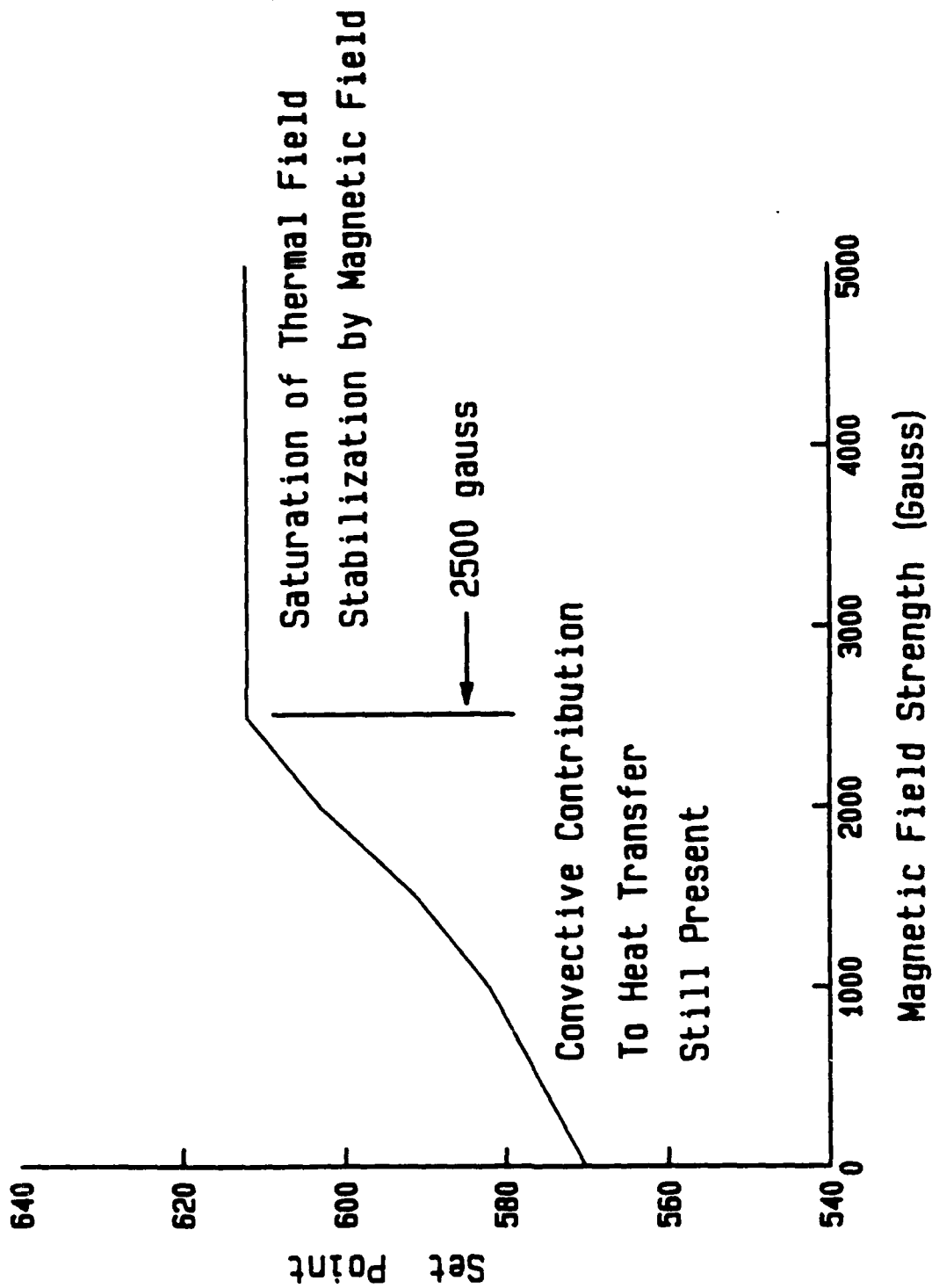
Magnetic Field Strength (Gauss)

Fig. 4.9   Effect of magnetic field on seeding setpoint in LP-LEC growth of GaAs.   Above 2500 gauss the melt is in the conduction-dominated heat transfer regime.   Mass transfer in the melt is still markedly influenced by the residual fluid flows.

transfer significantly, but have a noticeable impact on the redistribution of solute (impurities) in the melt and, consequently, in the resulting solid matrix.

CHARACTERIZATION

Efforts in GaAs characterization were directed toward establishing routine characterization captiblities: chemical etching, electrical measurements, and optical measurements. These standard approaches were analyzed for their ability to provide information which is quantitatively related to the growth process. Developmental efforts were directed toward the exploitation of the near infrared absorption and scattering properties of GaAs in conjunction with near infrared microscopy as an analytical tool to obtain information related to the structural and chemical perfection of grown bulk crystals.

Chemical Etching

Capabilities for etching 3-inch diameter GaAs in molten KOH [1] and molten NaOH:KOH eutectic [2] to reveal dislocation etch pits were established. Analysis of etch pit densities and distributions on undoped and Te-doped crystals indicates that the EPD $_{avg}$ is on the order of $10^4/cm^2$ with the density as much as one order of magnitude higher at the periphery (Fig. 4.10). Etch pit densities and distributions were obtained by counting along <110> directions on <100> oriented wafers cut perpendicular to the growth axis. The error associated with the counting process was evaluated by repeating the counting process on two wafers, along the same diameter.
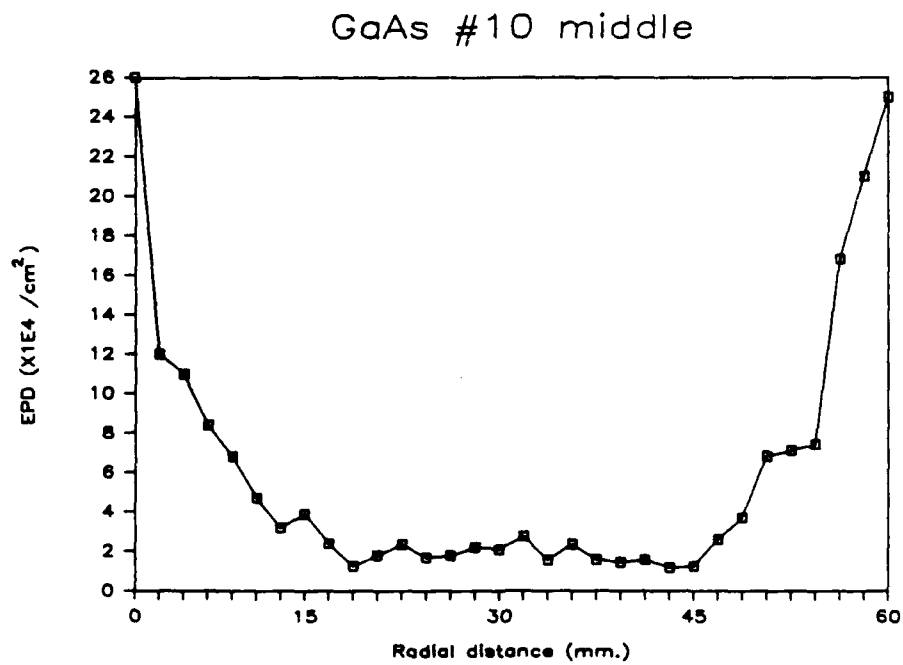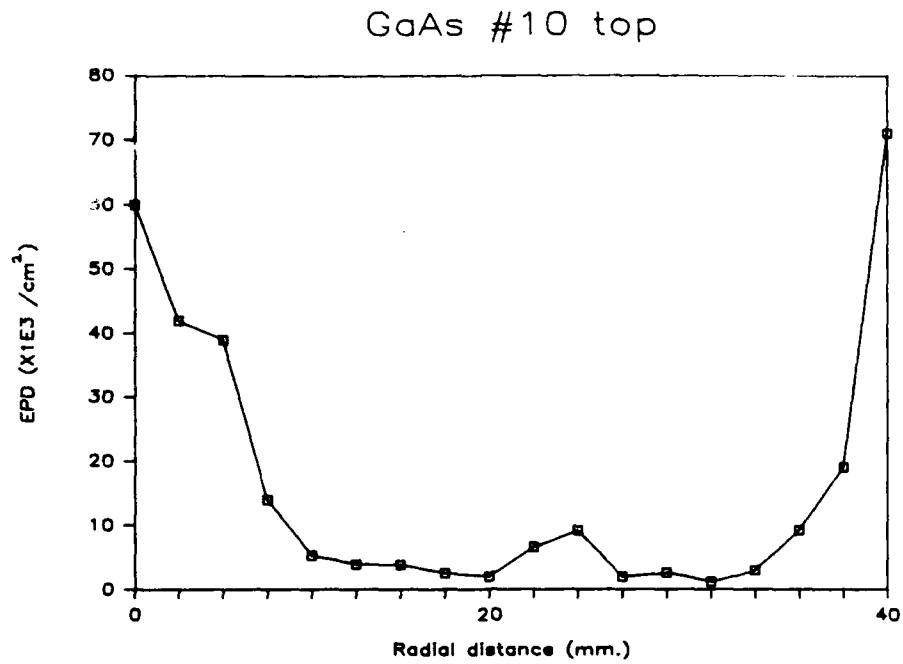
Fig. 4.10   Etch pit distribution for undoped LP–LEC GaAs crystal.

Errors associated with human etch pit counting were found to be between 15 and 30 percent. Doping with indium in the concentration range of $10^{19}/cm^3$ was ineffective in reducing the density of dislocation. Doping did bring about a transformation in the configuration for the dislocation network from one in which dislocations were polygonized (undoped and Te–doped crystals) to a situation in which dislocations are aligned within the primary slip system.

Capabilities in chemical etching for compositional variations was established. Two etchants were utilized: AB (CrO_3:HF:$AgNO_3$:H_2O) [3] and a photo–activated etch (H_2SO_4:H_2O_2:H_2O) [4]. Both etchants revealed surface features which could be interpreted as indicative of compositional variations. The etch features were obscured by extensive etching of defect structures. Qualitative observations of interface shapes of LP–MCZ crystals were possible. The interface shapes were observed to vary during growth from convex to sigmoidal to concave. The interface shapes observed were not reproducible from crystal to crystal, indicating that adequate control of heat transfer to and from the crystal had not been established.

Electrical Characterization

The Hall Effect, measured in the van der Paw configuration [5], was used to characterize the bulk transport properties of grown crystals. A comparison of data obtained from crystals grown with and without magnetic field melt stabilization indicates that significantly higher electron mobilities under conditions of higher net free

carrier concentrations are obtained in LP–MCZ crystals. The mechanism for this mobility increase is not understood, but could be related to (1) reduced scattering of electrons due to variations in the electric potential produced through increased compositional uniformity, or (2) reduced compensation levels, producing a reduced level of ionized impurity scattering.

Table 1
Comparison of Hall Data: Conventional vs. Magnetic LP–LEC

Sample	Field	Temp (K)	Carrier Conc. (cm^{-3})	Mobility
1	No	300	4.4×10^{15}	2000
2	No	300	1.7×10^{15}	2000
3	Yes	300	2.4×10^{17}	2500
4	Yes	300	3.0×10^{17}	2250

Optical Characterization

Optical characterization utilizing a Fourier spectrometer in the wavelength regime from 0.8–25 μm allowed the evaluation of two spectroscopic approaches to the analysis of compositional variations in grown crystals. Profiling of the free carrier concentration through the measurement of the absorption coefficient at 10 μm, and its interpretation within the framework of free carrier absorption, allows the calculation of the net free carrier concentration [6]. Data thus obtained for tellurium–doped

LP-MCZ crystals indicate that radial compositional variations are on the order of ±30% (Fig. 4.11). Due to the limited spatial resolution obtainable with this approach, microscale growth induced compositional variations (striations) could not be resolved.

The room temperature evaluation of the concentration and distribution of EL2 through the measurement of the absorption coefficient at 1 μm [7,8,9,10] was examined. We found that the evaluation of the concentration of EL2 by this method is unreliable in that the examined GaAs crystals exhibited significant variations in the baseline absorption level (Fig. 4.12). These baseline variations are tenatively attributed to variations in the density of scattering centers present in the crystal.

Near Infrared Microscopy

Near infrared transmission microscopy has for some time been recognized as a powerful tool for the analysis of structural and chemical inhomogeneities in GaAs. In indium- and selenium-doped LEC crystals cut parallel to the growth axis (Fig. 4.13) can be seen: growth striae due to fluctuations in the indium and selenium concentrations (both rotationally induced and non-rotational); screw dislocations; and lineage due to clusters of dislocations which were generated at the surface of the crystal propagating with growth. Efforts in the development of near infrared microscopy have been aimed at the quantification of the image formation mechanisms for features observed and the development of approaches to quantify the images obtained.
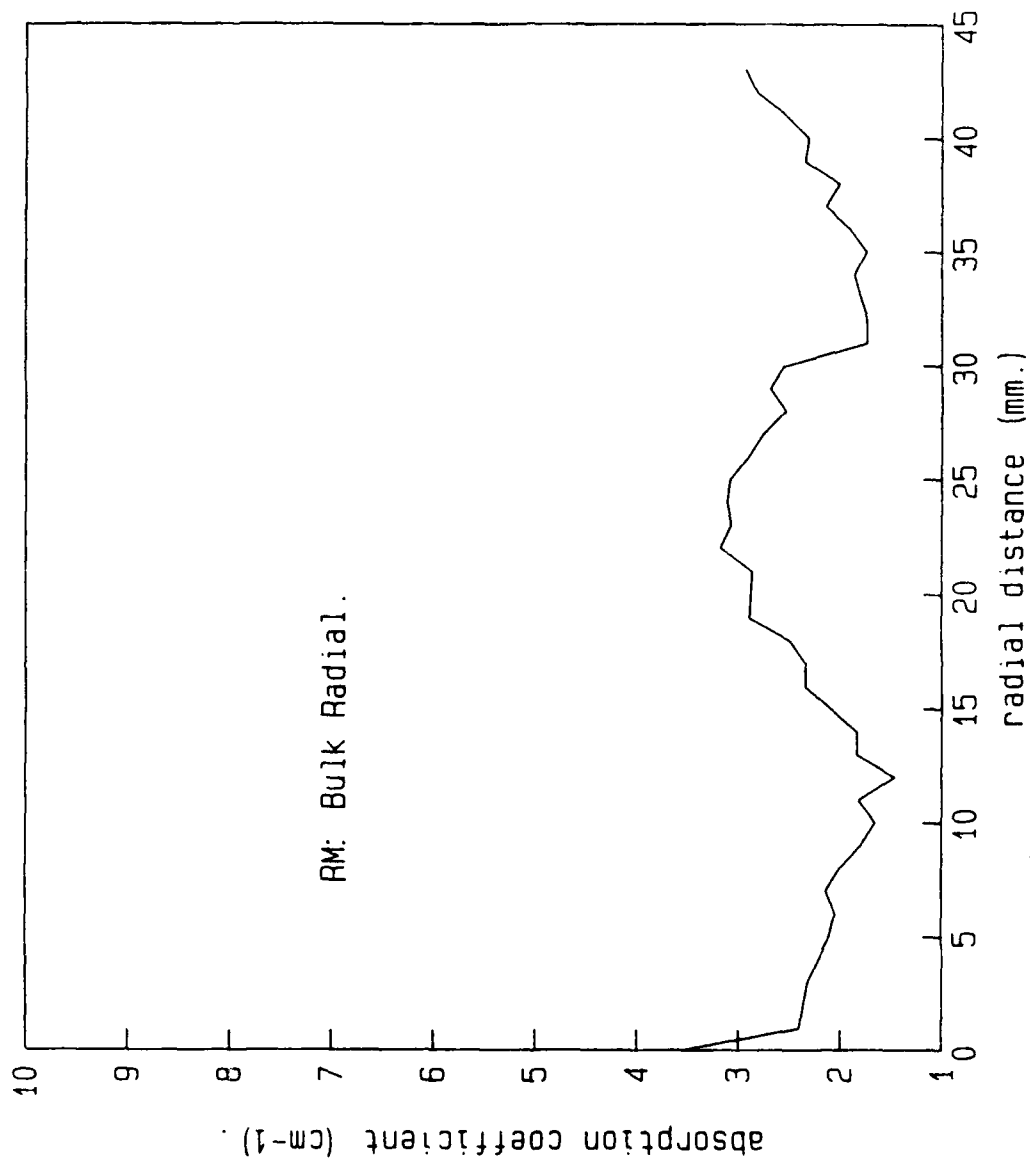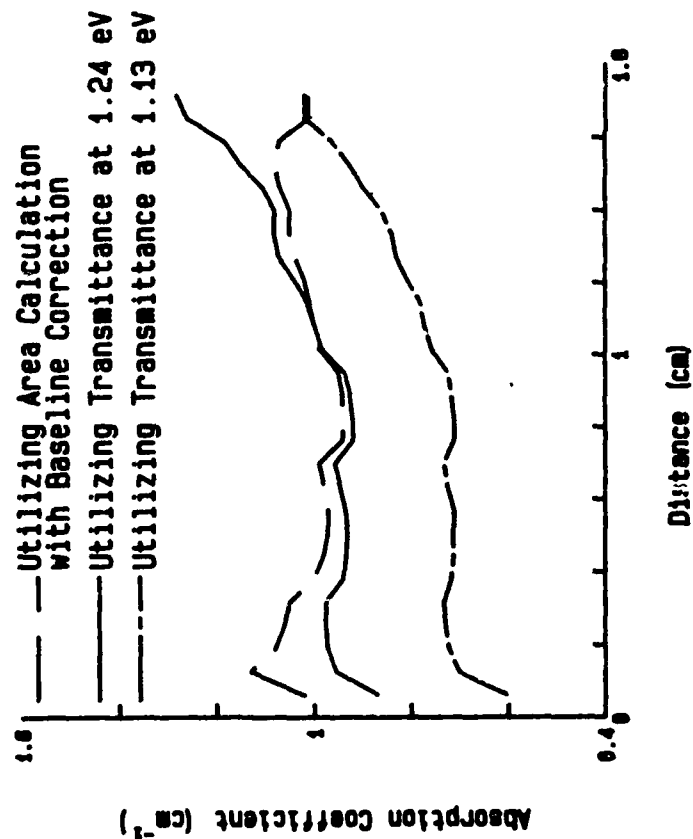
Fig. 4.11   Radial mid–IR (10 μm) absorption coefficient profile.

NIR Absorption along <110>

Across Radius of Undoped MCZ GaAs

(The Effect of Data Reduction Methods)

Absorbance Spectrum

Showing Data Reduction Methods

Radial Profiles

— — — Utilizing Area Calculation
with Baseline Correction

———— Utilizing Transmittance at 1.24 eV
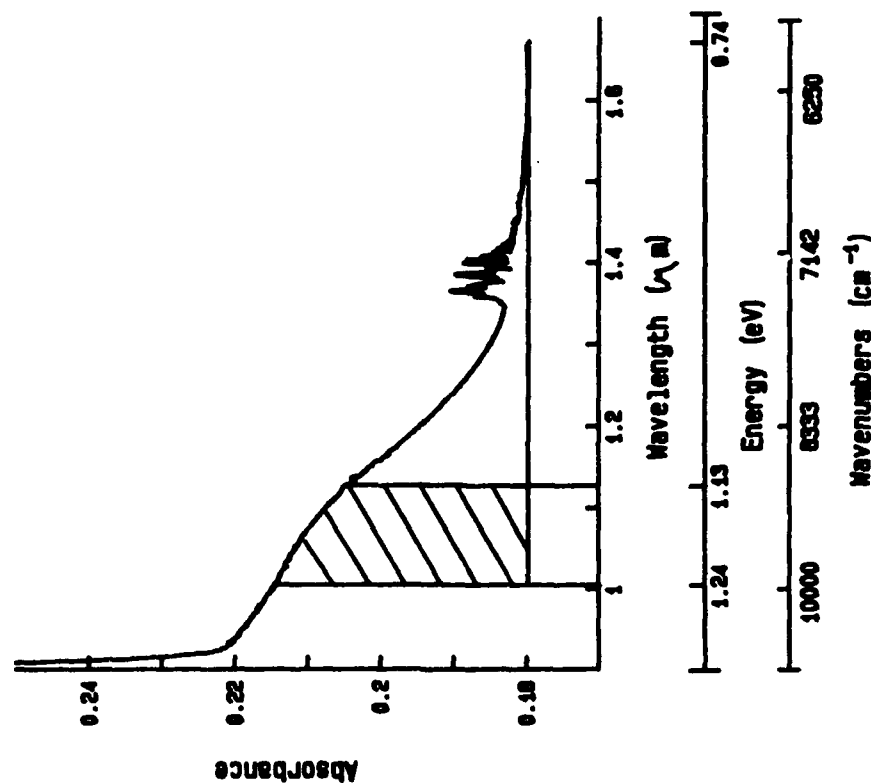
— ·— ·— Utilizing Transmittance at 1.13 eV

Fig. 4.12 The effect of data reduction methods for the determination of the concentration and distribution of EL2 from room temperature near infrared absorption measurements. If the variation in the "baseline" absorption of the crystal is not considered, variations in the absorption coefficient due to non-EL2 related phenomena can alter the determined profile.

Fig. 4.13   Near infrared micrograph of selenium— and indium—doped LEC GaAs
crystal. Observable in the micrograph are features which have been
identified as: (1) screw dislocations (down center of micrograph);
(2) growth—induced dislocations (converging on the center of the
image from the top and bottom); and (3) dopant striations (parallel
lines extending from the top to the bottom of the micrograph).

Image Formation:

The ability to image striae in NIR (near Infrared) transmission is not immediately obvious because shallow n–type dopants in GaAs exhibit their main optical activity in the mid–IR [6,11,12]. Two weak effects provide for image formation in the near infrared via an absorption phenomena. These two effects are:

1. a blurring or broadening of the band edge with increasing shallow impurity content [11], and

2. an increase in the absorption coefficient in the wavelength region of interest due to a shift in the "free carrier tail" with changing dopant (impurity) concentration.

Free carrier absorption in n–type crystals is a nondirect electronic transition involving electrons which are in the conduction band. Since this is a nondirect process, lattice scattering mechanisms must be considered when calculating the effect of free carriers upon the absorption of light. In the estimation of the effects of free carriers on image formation, the theoretical calculations of Walukiewicz et al. [6] appears logical. Accordingly, the contributions to the absorption coefficient by acoustic phonon scattering, screened optical phonon scattering, and ionized impurity scattering are considered. Thus, the absorption coefficient becomes:

$$\alpha_{tot}(\lambda) = \alpha_{op}(\lambda) + \alpha_{ac}(\lambda) + \alpha_{imp}(\lambda)$$

where in an approximation the contributions can be given by:

$$\alpha_{op, \lambda_1} = \alpha_{op, \lambda_0} \left(\frac{\lambda_1}{\lambda_0} \right)^{2.5}$$

$$\alpha_{ac, \lambda_1} = \alpha_{ac, \lambda_0} \left(\frac{\lambda_1}{\lambda_0} \right)^{1.5}$$

$$\alpha_{imp, \lambda_1} = \alpha_{imp, \lambda_0} \left(\frac{\lambda_1}{\lambda_0} \right)^{3.5}$$

Utilizing the wavelength dependence of free carrier absorption for two different net donor concentrations ($n = N_d - N_a$), theoretical calculations have been extended to the NIR. It is felt that these calculations provide a framework within which interpretation of the NIR image formation is possible. Note that these calculated values do not include the effects of compensation on the absorption coefficient. For GaAs with a moderate net donor concentration ($n = 1.0 \times 10^{16}$ cm^{-3}) the absorption coefficient is larger in the mid-ir and shows very little variation in the near infrared.

The sensitivity of the absorption coefficient at a given wavelength to the net donor concentration was calculated for wavelengths of 1 μm and 2 μm respectively. It is found that the greatest sensitivity in analysis is achievable by utilizing high net donor concentrations and mid-ir radiation.

Image Formation: Iso-electronic Dopants (In):

It is not evident that concentration variations of In dopant in GaAs produce contrast via absorption phenomena due to its electrical inactivity in the lattice. The only mechanism which can allow for an absorption effect is a large sensitivity to the band edge position with In concentration. This is not the case. Thus it is concluded that absorption phenomena are not a dominant mechanism for image formation in GaAs:In samples. Noted also is a contrast reversal of the image upon defocusing of the microscope. This is not observed in n-type samples where the contrast mechanism has been proposed to be due to an absorption effect. The image reversal leads to the hypothesis that the contrast generating mechanism in In-doped samples is due to an index of refraction change caused by lattice parameter variations with dopant concentration.

Fourier Analysis of Dopant Inhomogeneities in GaAs:

The ability to quantitatively examine relationships between growth parameters and the chemical uniformity of crystals on the microscale has been restricted to the segregation effects in elemental semiconductors through the application of spreading resistance measurements in conjunction with high resolution differential chemical etching [13]. Studies of dopant or impurity segregation in the growth of compound semiconductors has been restricted to qualitative interpretations of features found on chemically etched surfaces or the quantitative measurement of macroscopic bulk properties. As part of this research program, a technique based upon near infrared

microscopy has been developed which allows the rapid determination of dopant related optical properties on a microscale. Transmitted light intensity distributions which traverse growth striae are used to obtain the harmonic components contained in the dopant distribution through the application of Fourier analysis. This technique is applied to the examination of the degree of melt stabilization achieved through the application of a vertical magnetic field during LEC growth of InP and GaAs.

Sections cut parallel to the growth axis from n-type LEC grown InP and GaAs were lapped and polished optically flat on their front and back surfaces. The sections were placed on the stage of a standard transmission optical microscope fitted with an extended red Si-Vidicon camera (Fig. 4.14) to detect transmitted infrared radiation from the band edge of the given compound (corresponding to $\lambda=0.86$ μm for GaAs, $\lambda=0.93$ μm for InP) to 1.2 μm, or, alternately, a PbS-Vidicon camera can be used which extends the operation range of the optical system to 2.2 μm. The transmitted radiation, as detected by the video camera, is transferred to an image processing system which is resident in a high speed host computer. The incoming analog video signal is digitized in real time into a 512 by 512 pixel image with 256 (8-bit) gray level (light intensity) dynamic range. This data processing environment contains a series of digital image storage units allowing the rapid storage and manipulation of the incoming video signal. The manipulation of images is accomplished by a pipelined 16-bit pixel processor which allows for real time mathematical operations to be performed on in-coming video images. All image
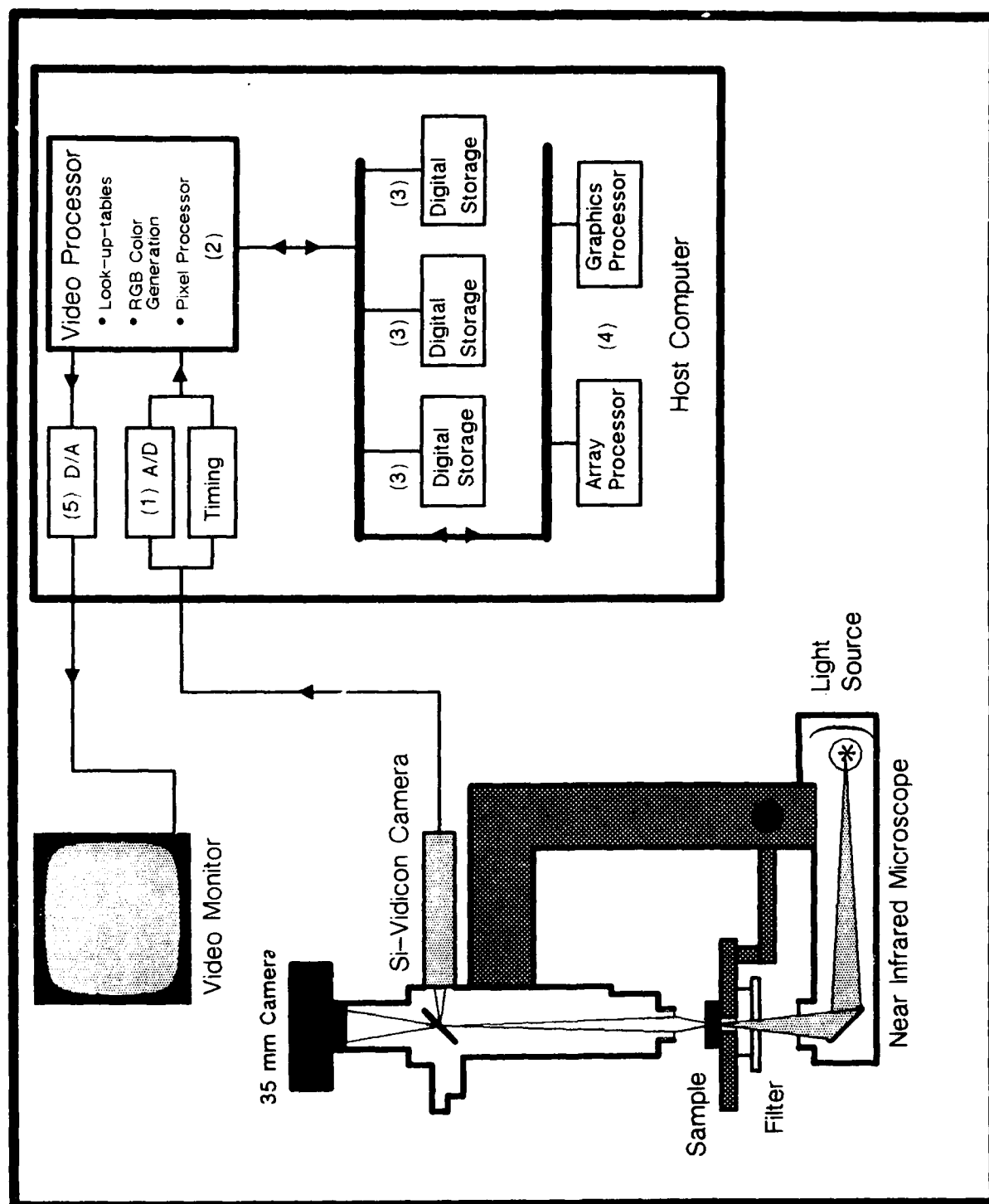
Fig. 4.14 Schematic of optical system and image processing system for Fourier analysis. The arrows indicate the direction of information flow through the system.

data in the processing unit are available, in parallel, to the host computer. Thus,

intensity data can, in real time, be read from the image and analyzed. In the

analytical approach taken, a linear pixel array traversing growth striae is read from the

image processing system and used as input to the host computer's array processor

where a real, discrete, fast Fourier transform is performed.

The acquired, user selected light intensity (gray level) distribution, $I(x)$, as a

bounded, discrete function can be analyzed for its harmonic content by performing a

real, discrete fast Fourier transform. As such:

$$I(x) = \frac{1}{2} \sum_n c_n e^{i\omega_n x}$$

where:

$$c_n = \frac{1}{L} \int I(x) e^{-i\omega_n x} dx$$

$$\omega_n = \frac{\pi n}{L}$$

In this representation, c_n as a function of ω_n is referred to as the "Fourier

Spectrum" of the function $I(x)$. The magnitude of c_n is indicative of the contribution

of a given harmonic, ω_n, to the original function (L is the fundamental period of the

function, in this case the distance along the sample from which the light intensity

distribution is obtained). Subsequent to performing the transform, the Fourier

spectrum, the light intensity distribution, and the near infrared transmission micrograph

are displayed simultaneously on a video display, or alternatively are available as hard copy.

Figure 4.15a depicts an infrared transmission micrograph of Sn-doped InP (n - 2×10^{18} cm^{-3} , 1-inch diameter). Superimposed upon this micrograph is a white line indicating the pixel array from which the light intensity distribution (Fig. 4.15b) has been obtained. This crystal was pulled at a rate of 1 cm/hr with seed rotation (15 RPM) and no crucible rotation. Under these growth conditions, the period of the expected rotational striae is 11 μm, corresponding to a frequency of 110 ω_0. Examination of the Fourier spectrum (Fig. 4.15c) reveals the absence of this frequency, yet the presence of 8 frequencies with a period longer than that of the rotational period. The data indicates that the dopant distribution in this crystal, grown without the application of a magnetic field, is dominated by uncontrolled, turbulent thermal n··'ural convection resulting in a seemingly chaotic dopant distribution. In qualitative agreement with theoretical estimations [14], it is also observed that low frequency perturbations dominate in their contribution to the observed dopant distribution.

The harmonic structure observed in crystals grown in the presence of a magnetic field is a function of both the magnetic field strength and prevailing rotation rates. A near infrared micrograph of a 3-inch-diameter tellurium-doped GaAs crystal (n - 1 by 10^{17} cm^{-3}) grown from a 2-kg melt contained within a 6-inch-diameter
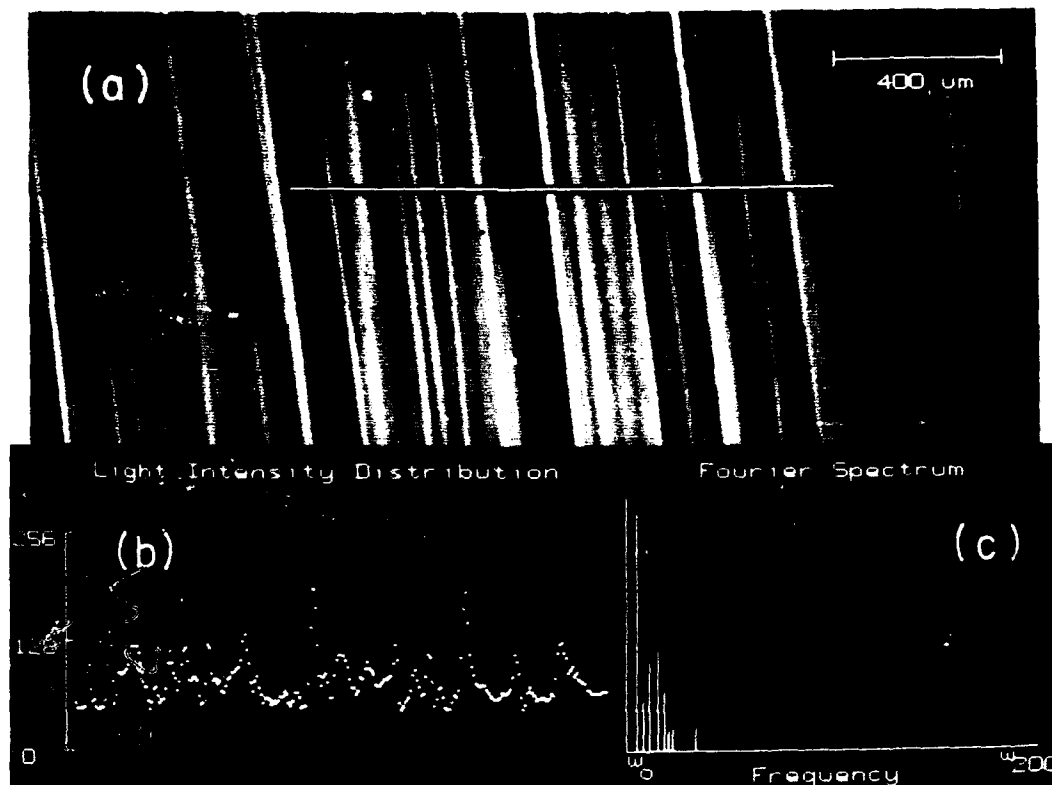
Fig. 4.15 Fourier analysis of tin–doped InP grown without magnetic field melt stabilization. The seemingly random distribution of striae is found to be comprised of low frequency harmonics, interpreted as the effect of turbulent melt flow on the distribution of the dopant.

crucible with a 1–kG axial magnetic field applied is presented in Fig. 4.16a. Rotation rates were 4 RPM seed rotation and –7 RPM crucible rotation. The lack of harmonic structure revealed by the Fourier transform (Fig. 4.16c) of the light intensity distribution (Fig. 4.16b) exhibits, surprisingly enough, a complete lack of periodicity in the dopant distribution which is as yet unexplained.

Results from a 3–inch–diameter tellurium–doped GaAs crystal grown with a 2 kG axial field applied under rotation rates of 8 RPM and 20 RPM for the seed and crucible respectively are presented in Fig. 4.17. The near infrared micrograph (Fig. 4.17a) exhibits a highly periodic striation pattern which is completely reflected in the transmitted light intensity distribution of Fig. 4.17b. The harmonic analysis of this distribution (Fig. 4.17c) indicates that only one frequency is present in the dopant distribution. This frequency corresponds to that expected from the imposed seed rotation rate, an indication that control over the dopant distribution has been achieved under these growth conditions.

The interpretation of the Fourier spectrum as an indication of the mode of dopant incorporation during the LEC growth of InP and GaAs is contingent upon an understanding of the possible causes of error in the analysis. This approach, based upon near infrared transmission microscopy, assumes that the dominant contribu on to the transmitted light intensity distribution is a result of the dopant. This contribution can be in the form of free carrier absorption in n– and p–type matrices as well as in
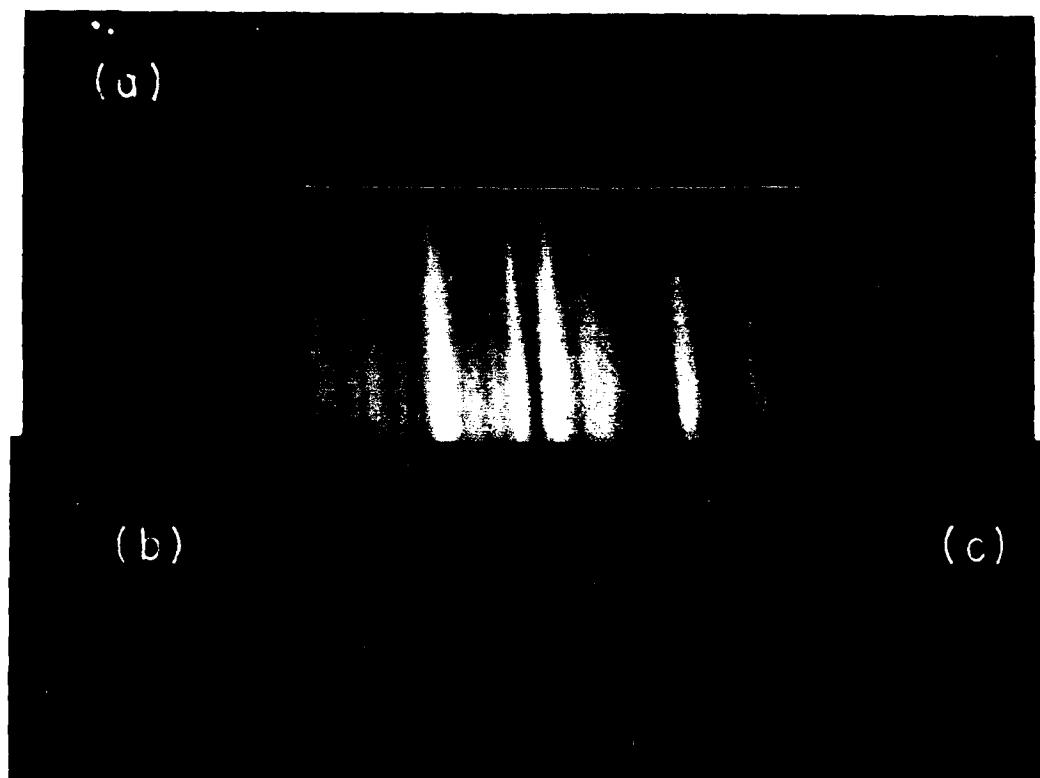
Fig. 4.16　Fourier analysis of Te–doped GaAs with partial magnetic field melt stabilization.　Note a complete absence of periodicity in the "Fourier spectrum".
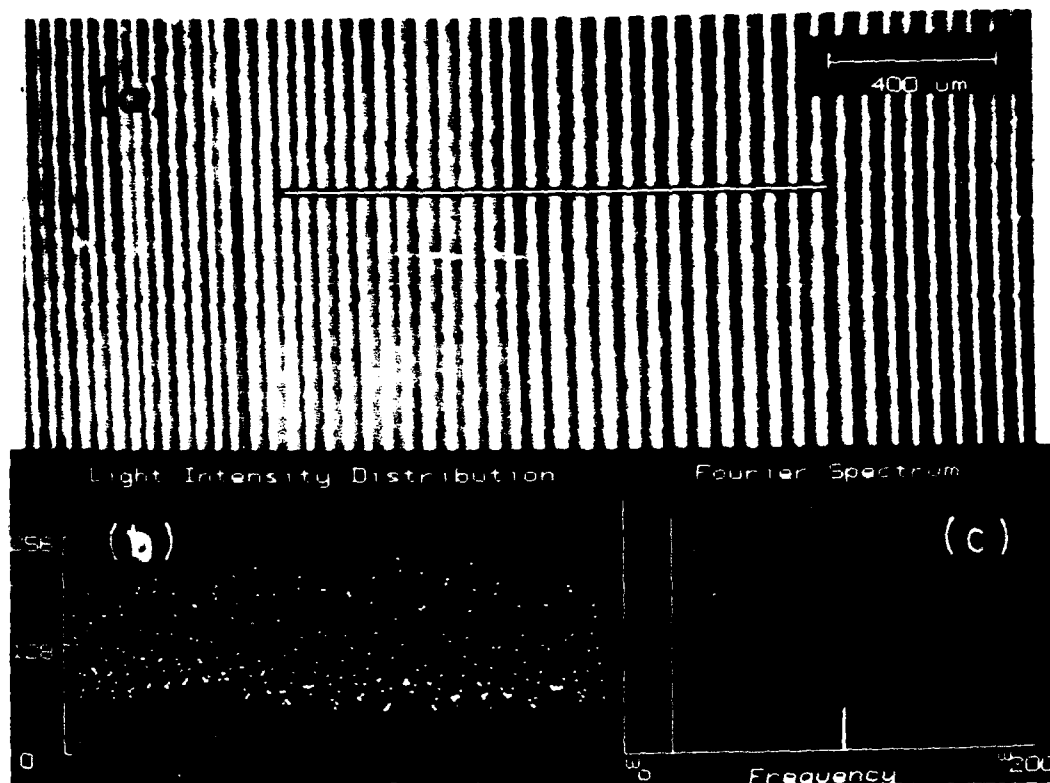
Fig. 4.17 Fourier analysis of Te-doped GaAs with magnetic field melt stabilization. The only harmonic present is directly related to the imposed seed rotation used during growth.

the form of refraction variations as in the case of indium–doped GaAs. For these

effects to dominate: (1) compensation effects must be negligible, and (2) the

sample must be free of scattering centers (precipitates, decorated dislocations). The

first condition is achieved by doping to a level high enough as to exceed the

background concentration of optically active impurities which are expected to be

present in the lattice. In the case of GaAs, contributions to the absorption coefficient

in the near infrared can arise due to EL2 at free carrier concentration ranges below

10^{17} cm^{-3}; thus, doping levels must be above this threshold to achieve an

unambiguous interpretation of the transmitted light intensity distribution as

corresponding to the dopant distribution. At this high dopant concentration level the

effect of compensation due to p–type impurities (e.g. carbon) can be considered as

negligible. Due to the image–based nature of this analytic approach, the effects of

scattering centers upon the transmitted light distribution can easily be evaluated

through an examination of the transmitted image. Further sources of error can be

introduced by the Fourier transform itself; no digital filtering of the output of the

transform is performed, hence aliasing of harmonic components to higher frequencies

is possible. Thus, the origin of high frequency harmonic components must be

carefully examined.

References

1. J.G. Grabmaier and C.B. Watson, Phys. Status Solidi 32, K13 (1969).

2. H. Lesoff and R. Gorman, J. Electronic Materials 13 (5) 733 (1984).

3.   M.S. Abrahams and C.J. Buiocchi, J. Appl. Phys. 36 (9) 2855 (1965).

4.   F. Kuhn–Kuhnefeld, J. Electrochem. Soc. 119 (8) 1063 (1972).

5.   L.J. van der Paw, Philips Res. Rpts. 13, 1 (1957).

6.   W. Walukiewicz, J. Lagowski, L. Jastrzebski, M. Lichtensteiger, and H.C. Gatos, J. Appl. Phys. 50 (2) 899 (1979).

7.   J.S. Blakemore and P. Dobrilla, J. Appl. Phys. 58 (1) 204 (1985).

8.   P. Dobrilla and J.S. Blakemore, J. Appl. Phys. 58 (1) 208 (1985).

9.   D.E. Holmes, R.T. Chen, K.R. Elliot, C.G. Kirpatrick, and P.W. Yu, IEEE Trans. Microwave Theory and Tech. MTT–30 949 (1982).

10. D.E. Holmes, R.T. Chen, K.R. Elliot, and C.G. Kirpatrick, Appl. Phys. Lett. 40 46 (1982).

11. J.I. Pankov, Optical Processes in Semiconductors, Dover, 1971.

12. W. Ulrici, Czech. J. Phys. B 34 420 (1984).

13. A.F. Witt, M. Lichtensteiger, and H.C. Gatos, J. Electrochem. Soc. 120 1119 (1971).

14. D.T.J. Hurle, J. Jakeman, and E.R. Pike, J. Crystal Growth, 3,4 633 (1969).